Edinburgh Research Explorer

Biochar and enhanced phosphate capture: Mapping mechanisms to functional properties

Published In:
Chemosphere

1 **Biochar and enhanced phosphate capture: mapping mechanisms to functional**

2 **properties**

3 Jessica Shepherd[1,2]*, Stephen Joseph[3,4], Saran Sohi[1,2], Kate Heal[1]

4 Affiliations

5 1) School of GeoSciences, University of Edinburgh, Alexander Crum Brown Road,

6 Edinburgh, UK EH9 3FF

7 2) UK Biochar Research Centre, University of Edinburgh, Alexander Crum Brown

8 Road, Edinburgh, UK EH9 3FF

9 3) School of Environmental and Life Sciences, University of Newcastle, Office C325,

10 Chemistry, Callaghan, New South Wales 2308, Australia

11 4) School of Materials Science and Engineering, University of New South Wales,

12 Kensington, NSW, Australia 2052

13 *Corresponding author

14

15 **Abstract**

16 A multi-technique analysis was performed on a range of biochar materials derived from

17 secondary organic resources and aimed at sustainable recovery and re-use of wastewater

18 phosphorus (P). Our purpose was to identify mechanisms of P capture in biochar and

19 thereby inform its future optimisation as a sustainable P fertiliser. The biochar feedstock

20 comprised pellets of anaerobically digested sewage sludge (PAD) or pellets of the same

21 blended in the ratio 9:1 with ochre sourced from minewater treatment (POCAD),

22 components which have limited alternative economic value. In the present study the

23 feedstocks were pyrolysed at two highest treatment temperatures of 450 and 550°C.

24 Each of the resulting biochars were repeatedly exposed to a 20 mg l^{-1} PO_4-P solution, to

25 produce a parallel set of P-exposed biochars. Biochar exterior and/or interior surfaces

26 were quantitatively characterised using laser-ablation (LA) ICP-MS, X-ray diffraction,

27 X-ray photo-electron spectroscopy (XPS) and scanning electron microscopy coupled

28 with energy dispersive X-ray. The results highlighted the general importance of Fe

29 minerals in P capture. XPS analysis of POCAD550 indicated lower oxidation state

30 Fe2p3 bonding compared to POCAD450, and LA-ICP-MS indicated stronger

31 covariation of Fe and S, even after P exposure. This suggests that low-solubility Fe/S

32 compounds are formed during pyrolysis, are affected by process parameters and impact

33 on P capture. Other data suggested subsidiary roles for aluminium, calcium and silicon.

34 Overall, our analyses suggest that a range of mechanisms for P capture are concurrently

35 active in biochar. We highlighted the potential to manipulate these through choice of

36 form and composition of feedstock as well as pyrolysis processing, so that biochar may

37 be increasingly tailored towards specific functionality.

38

39

1 Introduction

Freshwater and coastal ecosystems are at a high risk of damage caused by excess flows

of phosphate from land application and wastewater (Steffen et al., 2015). Concurrently

there is growing interest in the research, innovation and regulatory sectors to improve

the recovery and recycling of phosphate as agricultural fertiliser in response to predicted

future mineral phosphorus (P) scarcity (Reijnders, 2014). Traditional flocculation

techniques may not be effective for limiting P concentrations in wastewater discharges

to watercourses to reduce the risk of environmental damage to acceptable levels, for

example the 0.1 mg l^{-1} level proposed by Greenop and Wentworth (2014). Therefore,

alternative tertiary treatment methods are required, such as constructed wetlands

increasingly utilised in smaller wastewater treatment plants (WWTPs), using

combinations of plant, soil, and reactive materials to remove phosphate and nitrate to

prevent environmental damage downstream.

In order to recycle P from wastewater it is important that the materials used to recover P

are economic and the underlying mechanisms of P capture well understood. Low-cost,

bulk filter materials investigated to date include ochre, zeolite and blast furnace slags

(Cucarella et al., 2008; Dobbie et al., 2009; Drizo et al., 2006). The main mechanisms

of P capture in these systems are either chemisorption and precipitation by Fe or Al

(oxy)hydroxides, or precipitation with Ca (Arai and Sparks, 2001; Sakadevan and

Bavor, 1998). Activated carbons have also been developed for this purpose (Wang et

al., 2012), but the manufacture of these materials is more expensive than the direct recycling of secondary organic resources. A number of biochar materials, because of their similarities to activated carbon, have also been investigated. Biochars produced from anaerobically digested sugar beet tailings, digested sewage sludge and mallee tree (*Eucalyptus polybractea*) have all been shown to have phosphate capture functionality (Shepherd et al., 2016; Yao et al., 2011; Zhang et al., 2016), but most studies have involved either feedstock pre-treatment (Chen et al., 2011; Shepherd et al., 2016; Yao et al., 2011; Zhang et al., 2013, 2012) or post-treatment of the biochar (Li et al., 2016; Park et al., 2015; Ren et al., 2015; Zhang et al., 2016) to increase porosity and enrich the biochar with Mg, Al or Fe oxides.

Although many P sorption studies are reported in the literature, there is still no definitive model for biochar–phosphate interactions. Adding to the complexity of the system, many biochars have been shown to release, rather than capture phosphate into water and/or phosphate solutions (Angst and Sohi, 2013; Morales et al., 2013; Schneider and Haderlein, 2016). It has been suggested that phosphate may react with hydroxyl and carboxyl groups on the biochar surface (Laird and Rogovska, 2015) but such a reaction can only occur in the environment under extreme conditions or, in the case of biota, with the assistance of specialised enzymes (Gull et al., 2014). It is possible that the various phosphate anion species ($H_2PO_4^-$, HPO_4^{2-}, PO_4^{3-}) interact with C surfaces through hydrogen bonding and cation-mediated outer-sphere electrostatic interactions. These are weak compared to inner-sphere chemisorption and precipitation reactions which would occur with minerals, and thus are unlikely to be long-lived, unless in a relatively static system such as undisturbed soil. It has been suggested that adsorption of P by biochar will be dependent on the concentration and accessibility of

cations in the biochar ash fraction (Streubel et al., 2012). This is supported by reports of low affinity for P of low-ash biochar in aqueous solution (Hale et al., 2013; Morales et al., 2013; Yao et al., 2012). Even in biochar that has not been chemically modified, the identified mechanisms of P capture have been related to a native mineral ("ash") phase (Yao et al., 2011; Zhang et al., 2016), rather than functional carbon groups. The focus of subsequent optimisation of P capture properties has thus been on increasing the concentration and effectiveness of mineral phases on biochar surfaces. This can be likened to the research and development of activated carbon, where the activation step for improving P capture properties usually involves the addition of a metal reagent such as Fe or Zn (Bhatnagar and Sillanpää, 2011; Namasivayam and Sangeetha, 2004; Wang et al., 2012). Drawing on the general principles of coordination chemistry suggested by Streubel et al. (2012), we support a dominant role for minerals, but emphasise the mineral-carbon interface. The specific role of Fe, Al, Ca and Mg will vary with pH, as has been widely documented (Barrow, 1983; Goldberg and Sposito, 1985; Parfitt and Russell, 1977; Parfitt, 1989; Parfitt et al., 1975; Reddy et al., 1999; Sibrell et al., 2009; Torrent et al., 1992). This needs to be understood in the context of interface interactions.

In a previous study, we tested biochars made from a novel mix of anaerobically digested sewage sludge and ochre (Shepherd et al., 2016). The mix captured a greater amount of P from solution on a mass basis than activated carbon, ochre, or biochar from digested sludge only. To investigate the mechanisms underlying the P-capture function of that biochar we initiated the present study, with the overall goal of furthering the practical design of P capture materials in general. Consistent with this more practical context, we prepared new biochars using the original ingredients but pelletised before pyrolysis. We also used lower ochre content in mixed feedstock, namely 1:9 rather than 1:1 mass ratio. The surface properties were studied before and after exposure to aqueous P using a

115   range of spectroscopic and visualisation techniques. Our overarching hypothesis was

116   that P capture would be driven predominantly by mineral associations on surfaces and

117   less by functional carbon groups.

118

119   **2 Methods**

120   A summary of the materials, procedures and analyses used in this study and their

121   respective aims is given in Table 1. The biochars collectively encompass the range of

122   ochre (and therefore Fe), ash constituents and carbon components that allows the

123   relative contribution to P capture to be assessed. Characterisation was undertaken on

124   sub-samples with and without prior exposure to aqueous P solution, and of exterior

125   and/or interior surfaces of individual particles or pellets. Different characterisation

126   techniques covered different physical surface areas or surface thickness (i.e. sample

127   volume); they also provide information at different levels of detail, e.g. elemental

128   composition, functional groups, or oxidation state.

129

130   **2.1 Biochars**

131   **2.1.1 Non-pelletised biochars**

132   Biochars from non-pelletised feedstock were from the previous study (Shepherd et al.,

133   2016). They were produced in a small batch pyrolysis system at highest treatment

134   temperatures (HTTs) of 450 and 550°C. The feedstocks were anaerobically digested

135   sewage sludge (giving biochars AD450 and AD550) and the same sludge mixed with

136   ochre at a dry-mass ratio of 1:1 (giving biochars OCAD450 and OCAD550). These

137   relatively low HTTs were originally chosen so as to produce biochar with reactive sites

138   potentially related to carbon functional groups (Downie et al., 2009).

Table 1: Summary of the materials, analyses and their aims described in this study. First generation biochar materials AD450, AD550,

OCAD450, OCAD550 as well as ochre and activated carbon were characterised in Shepherd et al. (2016) and are indicated in italics. Elemental

concentrations of these materials determined previously by modified dry ashing/ICP-OES are outlined in Supplementary Information Tables S1

and S2. The pelletised materials were produced for this study and were characterised by the techniques listed above.

Material	Analyses							
	P capture and Release	**Correlation of P capture/element concentrations**	**Modified dry ashing/ICP-OES**	**pH and EC**	**XRD**	**XPS**	**LA-ICP-MS**	**SEM-EDX**
AD450	✓ *(previous work)*	✓	✓ *(previous work)*	✓ *(previous work)*	-	-	-	-
AD550	✓ *(previous work)*	✓	✓ *(previous work)*	✓ *(previous work)*	-	-	-	-
OCAD450	✓ *(previous work)*	✓	✓ *(previous work)*	✓ *(previous work)*	-	-	-	-
OCAD550	✓ *(previous work)*	✓	✓ *(previous work)*	✓ *(previous work)*	-	-	-	-
Ochre	✓ *(previous work)*	✓	✓ *(previous work)*	✓ *(previous work)*	-	-	-	-
Activated carbon	✓ *(previous work)*	✓	✓ *(previous work)*	✓ *(previous work)*	-	-	-	-
PAD450	✓ (capture only)	-	✓	✓	✓	-	-	✓
PAD550	✓ (capture only)	-	✓	✓	✓	-	-	✓
POCAD450	✓ (capture only)	-	✓	✓	✓	✓	✓	✓
POCAD550	✓ (capture only)	-	✓	✓	✓	✓	✓	✓
EPAD450	N/A	N/A	-	-	✓	-	-	✓
EPAD550	N/A	N/A	-	-	✓	-	-	✓
EPOCAD450	N/A	N/A	-	-	✓	✓	✓	✓
EPOCAD550	N/A	N/A	-	-	✓	-	✓	✓
Mechanistic and chemical information obtained	Determination of P capture/release characteristics	Effect of elemental composition on P capture and release	Effect of feedstock, processing and/or pyrolysis conditions and pyrolysis HTT on elemental composition	Effect of feedstock, processing and/or pyrolysis conditions and pyrolysis HTT on pH and EC	Effect of feedstock, pyrolysis HTT and P exposure on mineral phases	Effect of P exposure on surface and whole properties	Effect of pyrolysis HTT and P exposure on surface properties	Effect of feedstock, pyrolysis HTT and P exposure on surface properties
Biochar nomenclature	AD – Anaerobically digested sewage sludge OCAD – 50% Minto ochre and AD mixture (pre-pyrolysis) PAD – Pelletised Anaerobically digested sewage sludge POCAD – Pelletised 10% Minto ochre and AD mixture (pre-pyrolysis)				EPAD – P exposed PAD biochar EPOCAD – P exposed POCAD biochar 450 – 450°C highest treatment temperature (HTT) for pyrolysis 550 – 550°C highest treatment temperature (HTT) for pyrolysis				

143   **2.1.2 Pelletised biochars**

144   Biochars were made from pelletised feedstocks using a bench-scale continuous

145   pyrolysis unit. It is more practical to pelletise feedstock than biochar; screw-feeders

146   used in scalable, continuous flow pyrolysis systems also perform best with feedstock in

147   pelletised form. The digested sewage sludge and ochre were sourced from the same

148   locations as in the previous study. Anaerobically digested sewage sludge (50 kg wet

149   mass) was sampled from the Newbridge WWTP (Edinburgh, Scotland) and oven dried.

150   Ochre was obtained from the Minto minewater treatment plant (Fife, Scotland) and

151   sieved to < 1 mm. Pellets were prepared from the sludge and/or ochre and a

152   lignocellulose binder agent in the ratios 89.1:9.9:1.0 and 99.0:0:1.0. The mixtures were

153   passed through a die to form pellets approximately 0.5 cm diam. × 2 cm in length. The

154   pellets were pyrolysed at the UK Biochar Research Centre (UKBRC) using the bench-

155   scale continuous flow unit described previously (Buss et al., 2016a). The HTTs used in

156   the previous study (Shepherd et al., 2016) were used to produce the four new biochar

157   materials: PAD450, PAD550, POCAD450 and POCAD550.

158

159   **2.1.3 P–exposed pelletised biochars**

160   To investigate the mechanisms of P capture on biochar surfaces, pelletised biochars

161   defined above were exposed to aqueous P using a MOPS-buffered (3-(N-morpholino)

162   propanesulfonic acid, Sigma Aldrich, St Louis, MI) K_2HPO_4 solution containing

163   20 mg P l^{-1}, following the procedure described previously (Shepherd et al., 2016)

164   modified as described here. Each biochar (30 g, PAD450, PAD550, POCAD450 and

165   POCAD550) was used to provide representative particles of the physically

166   heterogeneous samples, selecting only particles of diameter 0.25–15 mm. The P

167   solution was added in a 1:20 solid to liquid ratio (m/v) and shaken with the biochar for

168 24 h. After this time the solution was poured off from the biochar and replaced with

169 fresh P solution. This was repeated for 6 days to ensure sufficient uptake of P on the

170 external surfaces of the biochar to analyse using the chosen techniques. At the end of

171 each 24 h treatment two samples of the solution were analysed colorimetrically (Auto

172 Analyser III, Bran & Luebbe, Norderstedt, Germany) to determine the amount of P

173 captured by the biochars. The P-exposed samples were designated EPAD450,

174 EPAD550, EPOCAD450 and EPOCAD550.

175

176 **2.2 Characterisation**

177 **2.2.1 pH – pelletised biochars**

178 To provide insights on surface protonation of pelletised biochars, the pH of crushed

179 samples was determined in duplicates for PAD450, PAD550, POCAD450 and

180 POCAD550, in DI water using the method recommended by the International Biochar

181 Initiative (IBI).(IBI, 2012)

182

183 **2.2.2 P capture and release – non-pelletised biochars**

184 P-capture and release dynamics of the non-pelletised biochars (AD450, AD550,

185 OCAD450 and OCAD550) were described and reported in the previous study

186 (Shepherd et al., 2016). It is the statistical analysis of the results in the light of new

187 characterisation data that is the main focus of the present study. Briefly, replicate (n = 4)

188 1.0 g samples of each biochar, the ochre and an activated carbon (Sigma Aldrich, St

189 Louis, MI) were repeatedly exposed for 24 h repeated over 5 days to 20 ml solutions of

190 either 20 or 800 mg l^{-1} P (from K_2HPO_4, Sigma Aldrich, St Louis, Missouri, USA)

191 buffered at pH 7 using MOPS and $NaNO_3$ as a background electrolyte. To test the

192 release of the captured P, the P-enriched materials were then exposed to pH 7 MOPS-

193 buffered deionised (DI) water for 24 h repeatedly over 4 days.

194

195 **2.2.3 Bulk elemental composition – pelletised and non-pelletised biochars, ochre**

196 **and activated carbon**

197 Samples were digested prior to ICP-OES analysis using the modified dry ashing method

198 (Enders and Lehmann, 2012), as per published modifications (Buss et al., 2016b;

199 Shepherd et al., 2016). Briefly, 0.5 g samples were taken from sub-sampled and crushed

200 materials, ashed in a muffle furnace then digested in HNO_3 and HCl. The materials and

201 blanks were digested in triplicate and ICP-OES elemental quantification was performed

202 using a Perkin Elmer Optima 5300DV instrument (Waltham, USA). Most elements

203 were analysed in axial mode, except for Al, Ca, Fe, K, Mg and Na, which were present

204 in sufficient concentrations to necessitate the use of radial mode. Standards were run

205 with each analysis session for calibration and to check the accuracy of measurements

206 over the time of the sample run. The limit of detection for each element was determined

207 using an existing method (Buss et al., 2016b).

208

209 **2.2.4 X-ray diffraction (XRD) – pelletised biochars**

210 Cobalt Kα XRD was performed in duplicate on PAD450, PAD550, POCAD450,

211 POCAD550, EPAD450, EPAD550, EPOCAD450 and EPOCAD550 using an

212 Empyrean thin-film XRD (PANalytical, Almelo, the Netherlands). Analyses were

213 initially attempted using standard Cu Kα XRD, but confounded by the large background

214 signal from amorphous carbon phases.

215

216 **2.2.5 X-ray photoelectron spectroscopy (XPS) – pelletised biochars**

217 Surface layer functional groups and elemental composition was examined for one

218 randomly sampled pellet fragment of POCAD450, EPOCAD450 and POCAD550.

219 Mono-chromated Al Kα XPS was applied using an ESCALAB250Xi instrument

220 (Thermo Scientific, Waltham, MA). The analysis parameters were as follows: 1486.68

221 eV photon energy, 150 W power and spot size of 500 μm. The core level binding

222 energies (BEs) were aligned with C1s peak BE of 285.0 eV. Data were analysed with

223 Avantage software (Thermo Scientific, Waltham, MA). The surfaces of POCAD450

224 and EPOCAD450 pellets were analysed to identify differences in properties before and

225 after P exposure, respectively. Surfaces of POCAD550 were also analysed to identify

226 whether pyrolysis HTT had an effect on surface composition in these biochars. To gain

227 an insight as to the effect on pellet size on the utilised capacity for P interaction

228 measurements were also conducted on interior surfaces of the analysed POCAD and

229 EPOCAD, exposed by crushing the pellet.

230

231 **2.2.6 Laser ablation-ICP-MS – pelletised biochars**

232 To study the relationship between P and other elements on the surface of P-exposed and

233 non-treated biochar to a depth of 5 μm, elemental analysis by laser ablation (LA) ICP-

234 MS was used. The analysis was applied to a randomly selected pellet of each of

235 POCAD450, POCAD550, EPOCAD450 and EPOCAD550 using a NWR213 Laser

236 Ablation unit (ESI New Wave, Portland, OR) coupled to a NexION 300D ICP-MS

237 (Perkin Elmer, Waltham, MA). Laser ablation parameters were as follows: wavelength

238 213 nm, repetition frequency 10 Hz, laser energy density 0.48 J cm^{-2} (at 30%), spot size

239 110 μm and scan speed 20 μm s^{-1}. ICP-MS was performed at Rf power of 1150 W,

240 helium gas flow rate of 0.8 l min^{-1}, argon gas flow rate of 0.6 l min^{-1}, in peak hopping

241 scan mode and with a dwell time of 0.05 s. NIST610 and NIST612 glass standards were

242 used to estimate the elemental concentrations of the biochar obtained in three separate

243 2 mm line scans for each pellet (resulting in between 219 and 223 sample locations for

244 each pellet).

245

246 **2.2.7 Scanning electron microscopy with energy-dispersive X-ray spectroscopy**

247 **(SEM-EDX)**

248 SEM-EDX analyses were performed on all P-exposed and non-exposed biochars

249 (PAD450, PAD550, POCAD450, POCAD550, EPAD450, EPAD550, EPOCAD450

250 and EPOCAD550) to a depth of approximately 6 μm. Data was gathered using Nova

251 Nano SEM 230 and 450 field-emission scanning electron microscopes (FEI, Hillsboro,

252 OR), each configured with a Bruker silicon drift detector energy dispersion X-ray

253 spectrometer (Bruker, Billerica, MA), as well a Sigma SEM (Zeiss, Jena, Germany).

254 Samples were sputter coated with chromium prior to analysis. The resolution of EDX

255 scans was 6 μm. To encompass as many P phases as possible, the whole region was

256 quantified; many P phases have a dimension in the μm range. Elemental mapping

257 provided by EDX was used to visualise the association of P and other elements in

258 support of the other analyses.

259

260 **2.3 Statistical analysis**

261 **2.3.1 Correlation of biochar element concentration and P capture and release –**

262 **non-pelletised biochars**

263 To identify whether specific elements were associated with P capture or release, mean P

264 capture and release results (n = 6) were correlated against the concentration of 19

265 elements in AD450, AD550, OCAD450, OCAD550, ochre and activated carbon

266 determined as described in 2.2.3. The cumulative results for 1 and 5 days x 20 mg l^{-1} P

267 repeated exposure and 1 and 4 days x treatments for P release as described in section

268 2.2.2 were used. Pearson's product-moment correlation coefficients were calculated

269 since all data were found to be normally distributed by the Shapiro-Wilk test. Where

270 element concentrations were below the limit of detection for two or more of the

271 materials (i.e. resulting in n < 4), the element was excluded from the analysis. RStudio

272 (RStudio Team, 2015) was used for all statistical analyses, with significance indicated

273 by $p < 0.05$.

274

275 2.3.2 Analysis of Laser ablation ICP-MS results

276 Correlation analysis between P and other elements measured by LA-ICP-MS was

277 performed using the approach described in 2.3.1, with Spearman's rho calculated where

278 one or both sets of data were not normally distributed. To further interpret elemental

279 composition on biochar surfaces, we applied Principal Component Analysis (PCA) to

280 the results for each sample location using the prcomp function in RStudio (RStudio

281 Team, 2015) with data centring, scaling and specifying a tolerance of 0.3 to filter out

282 noise and thereby limit the number of identified principal components. PCA provides

283 insights into elemental clustering as well as the localisation of P on sample surfaces

284 before and after exposure to P solution.

285

286 3 Results

287 3.1 Bulk properties

288 3.1.1 Elemental composition

289 The lower content of ochre in the POCAD feedstock compared to OCAD (10 vs 50%)

290 explained some differences in nutrient concentrations between PAD and POCAD

291 (Table 2) compared to their non-pelletised analogues (AD and OCAD). In general, the

292 non-pelletised biochars appeared to show greater elemental loss on a mass basis,

293 compared to their feedstocks, than for the pelletised biochars (See Supplementary

294 Tables 1 and 2 for more detail). Calcium and P present in the feedstocks was retained to

295 a higher extent in the pelletised biochars, suggesting that either pelletisation and/or the

296 continuous flow bench scale pyrolysis process provides conditions less conducive for

297 volatilisation of Ca and P than small scale batch pyrolysis.

298

299 The main difference between the PAD and POCAD biochars was in the concentration

300 of Fe, reflecting feedstock composition (see Table 3). The incorporation of 10% ochre

301 (dry weight) to the feedstock resulted in a Fe concentration in POCAD twice that of

302 PAD. Despite similar concentrations in PAD and POCAD feedstocks, POCAD

303 contained relatively less Cr than PAD at both HTTs (24.9 ± 0.880 and 21.1 ± 1.16 mg g^{-}

304 ^{1} for POCAD vs 33.8 ± 1.25 and 30.1 ± 0.538 mg g^{-1} for PAD) (mean $\pm$ 1 standard

305 deviation, n = 3). Compared to the non-pelletised biochars, the PAD and POCAD

306 biochars contained more Al, Cr, Cu, Mo, Na, Ni and Zn, but less B and Co. The lower

307 Co concentration reflects a lower concentration in the feedstock, but this is not the case

308 for B, which may have also been lost during digestion in the modified dry ashing

309 process. The concentrations of Mo and Na in the pelletised feedstocks are higher than in

310 non-pelletised, explaining part of the difference in concentration in the biochars. In

311 addition, there is considerably more Cr, Cu and Zn in POCAD than OCAD, probably

312 from contamination of feedstock during the pelletisation process. Overall, the data

313 indicate that pelletisation and/or continuous flow pyrolysis favours greater retention of

314 some elements in biochar. The pH of the pelletised biochars ranged from 7.39 to 8.25,

315 which is slightly higher than for the non-pelletised analogues. This is likely to be related

316 to the relative retention of salts discussed above.

317 *Table 2: Mean nutrient concentrations (n=3) of the materials as determined by ICP-OES of sample digests expressed in g kg^{-1} ± 1 standard*

318 *deviation. See Table 1 for sample nomenclature.*

319

	PAD	Ochre	POCAD	PAD450	POCAD450	PAD550	POCAD550
Yield %	-	-	-	29.4	38.7	37.9	38.0
pH (n=2)	-	7.9 ± 0.014	-	7.49 ± 0.02	7.39 ± 0.05	8.25 ± 0.08	7.85 ± 0.03
EC (µS cm^{-1}) (n=2)	-	518 ± 20	-	TBC	TBC	TBC	TBC
Nutrients (g kg^{-1}) n=3							
Ca	28.7 ± 0.569	18.8 ± 0.438	28.8 ± 0.400	59.9 ± 1.98	58.1 ± 0.534	62.0 ± 1.06	53.9 ± 1.08
K	2.53 ± 3.99×10^{-2}	0.349 ± 4.76×10^{-2}	2.10 ± 2.69×10^{-2}	5.09 ± 0.142	4.59 ± 6.75×10^{-2}	5.51 ± 6.61×10^{-2}	4.20 ± 0.125
Mg	5.12 ± 7.96×10^{-2}	3.03 ± 5.88×10^{-2}	5.09 ± 5.79×10^{-2}	10.4 ± 0.281	10.5 ± 0.107	10.8 ± 0.138	9.52 ± 0.209
Mn	0.142 ± 0.149×10^{-2}	0.891 ± 5.33×10^{-3}	0.183 ± 0.278×10^{-2}	0.327 ± 0.881×10^{-2}	0.373 ± 0.528×10^{-2}	0.336 ± 0.969×10^{-2}	0.357 ± 0.856×10^{-2}
P	52.1 ± 9.62×10^{-2}	1.92 ± 0.134	51.5 ± 0.561	109 ± 3.08	103 ± 1.95	114 ± 1.19	98.7 ± 1.73
S	9.82 ± 0.425	3.32 ± 0.121	8.81 ± 0.160	16.8 ± 0.406	18.1 ± 0.279	16.3 ± 0.203	16.6 ± 0.217

Table 3: Mean potentially toxic element concentrations (n=3) of the materials as determined by ICP-OES of sample digests expressed in mg kg^{-1} ± 1 standard deviation. See Table 1 for sample nomenclature.

	PAD	Ochre	POCAD	PAD450	POCAD450	PAD550	POCAD550
Al	$23.6 \times 10^3 \pm 121$	$2.09 \times 10^3 \pm 227$	$22.7 \times 10^3 \pm 151$	$46.5 \times 10^3 \pm 953$	$46.6 \times 10^3 \pm 354$	$49.5 \times 10^3 \pm 666$	$43.4 \times 10^3 \pm 1130$
As	< 0.72	< 0.72	< 0.72	< 0.72	< 0.72	< 0.72	< 0.72
B	$9.26 \pm 9.28 \times 10^{-2}$	43.8 ± 6.09	15.3 ± 3.46	18.6 ± 0.428	19.8 ± 1.49	18.0 ± 0.159	16.1 ± 0.407
Cd	$0.281 \pm 1.77 \times 10^{-2}$	< 0.04	< 0.04	$1.77 \pm 4.33 \times 10^{-2}$	$0.169 \pm 1.05 \times 10^{-2}$	$1.15 \pm 9.33 \times 10^{-2}$	$0.322 \pm 8.54 \times 10^{-2}$
Co	2.94 ± 0.264	$9.65 \pm 5.98 \times 10^{-2}$	$3.10 \pm 5.52 \times 10^{-2}$	6.05 ± 0.139	6.71 ± 0.119	6.30 ± 0.167	6.10 ± 0.190
Cr	11.8 ± 0.233	< 0.49	10.6 ± 0.674	33.8 ± 1.25	24.9 ± 0.880	30.1 ± 0.538	21.1 ± 1.16
Cu	44.0 ± 1.18	< 0.06	39.1 ± 0.572	110 ± 1.54	103 ± 2.10	112 ± 7.67	98.9 ± 3.70
Fe	$38.9 \times 10^3 \pm 719$	$520 \times 10^3 \pm 7.44 \times 10^3$	$77.0 \times 10^3 \pm 2.51 \times 10^3$	$80.8 \times 10^3 \pm 2.93 \times 10^3$	$130 \times 10^3 \pm 2.00 \times 10^3$	$84.5 \times 10^3 \pm 1.53 \times 10^3$	$130 \times 10^3 \pm 1.92 \times 10^3$
Mo	10.9 ± 0.556	< 0.21	12.5 ± 0.942	21.9 ± 0.459	26.7 ± 0.620	23.8 ± 0.756	24.3 ± 0.287
Na	$5.11 \times 10^3 \pm 274$	$1.86 \times 10^2 \pm 30.3$	$1.33 \times 10^3 \pm 44.4$	$9.90 \times 10^3 \pm 219$	$5.23 \times 10^3 \pm 48.5$	$10.5 \times 10^3 \pm 208$	$3.75 \times 10^3 \pm 171$
Ni	7.14 ± 0.549	$5.90 \pm 7.79 \times 10^{-2}$	7.23 ± 0.178	29.4 ± 0.895	$23.0 \pm 9.81 \times 10^{-2}$	26.3 ± 0.889	18.8 ± 0.420
Pb	11.8 ± 0.362	10.1 ± 0.824	13.2 ± 1.77	31.9 ± 4.23	25.1 ± 0.351	29.8 ± 0.771	28.3 ± 3.72
Zn	360 ± 4.75	60.6 ± 0.985	350 ± 2.71	787 ± 9.68	746 ± 6.50	825 ± 15.8	706 ± 12.4

3.1.2 Phosphorus exposure of the pelletised biochars

Repeated exposure of biochars to 20 mg P l^{-1} MOPS-buffered solution resulted in P

capture of 0.57 ± 0.26 mg P g^{-1} for PAD450 (mean $\pm$ 1 standard deviation, n = 2),

0.70 ± 0.40 mg P g^{-1} for PAD550, 0.95 ± 0.18 mg P g^{-1} for POCAD450 and

0.95 ± 0.23 mg P g^{-1} for POCAD550. The P capture by non-pelletised biochars AD and

OCAD(Shepherd et al., 2016) were higher: $0.99 \pm 9.3 \times 10^{-3}$ mg P g^{-1} to $1.3 \pm 4.7 \times 10^{-3}$

mg P g^{-1}. This may be attributed to the larger size of analysed pellet fragments (0.25–15

mm) compared to crushed particles (0.5–1.0 mm) i.e. a surface area effect.

3.1.3 Elemental associations in P capture and release for non-pelletised biochars

The significant correlations between P capture and release and bulk element

concentrations are shown for AD450, AD550, OCAD450, OCAD550, ochre and

activated carbon in Table 4. After 1 day (1 x 24 h) exposure to a 20 mg P l^{-1} solution, P

capture from solution was correlated negatively and strongly significantly with biochar

Al, Cu, K, Na and Zn concentration. After 5 days (5 x 24 h) of exposure only Pb was

significantly correlated (negatively), although Pb concentration of the materials was

also very low ($< 3.2 \times 10^{-3}$ g kg^{-1}). After 5 days, P capture was positively and strongly

significantly correlated with Fe, which was present in biochar at 44.6–451 g kg^{-1}.

In terms of P release following P exposure, after 1 day shaking in MOPS-buffered pH 7

DI water, P release was significantly negatively correlated with Fe, suggesting that

higher Fe content is associated with lower solubility of captured P at pH 7. After 4 days

the negative correlation with Fe was no longer significant, but P release was

significantly positively correlated with both initial biochar Cu and Na concentration,

346 indicating that these elements may be present in P compounds of greater solubility after

347 P capture.

348

349 *Table 4: Pearson's product-moment correlation coefficients for elements where a*

350 *statistically significant correlation between elemental concentration and P capture or P*

351 *release was determined (n = 6) at the start or end of the experiments for the first*

352 *generation materials (AD450, OCAD450, AD550, OCAD550, ochre and activated*

353 *carbon) using a 20 mg P l^{-1} solution reported in Shepherd et al. (2016). * = p < 0.05,*

354 *** = p < 0.01, *** = p < 0.001*

	P capture		P release	
	Day 1	Day 5	Day 1	Day 4
Al	-0.886*	-0.412	-0.194	0.0916
Cu	-0.961**	-0.478	0.642	0.860*
Fe	0.605	0.878*	-0.858*	-0.740
K	-0.850*	0.465	0.528	0.748
Mn	0.194	0.711	-0.609	-0.382
Na	-0.967**	-0.521	0.664	0.879*
Pb	-0.292	-0.887*	0.786	0.536
Zn	-0.854*	-0.358	0.487	0.730

361

362

3.1.4 Mineral phases identified by X-ray diffraction

364 Due to the presence of amorphous C in the pelletised biochars, few mineral elements

365 were identified, even using the Co method (Table 5). The analysed biochars all

366 contained SiO_2 (quartz). Other detectable minerals were mostly complex silicates

367 containing different combinations of Al, Ca, K, Mg, Mn and Na. The only phosphate-

368 containing mineral detected was Al phosphate in EPOCAD450. Interestingly, no iron

369 minerals were identified, indicating that Fe is either amorphous or present in a diversity

370 of crystalline forms at very low individual concentrations.

371

372   *Table 5: Minerals detected in the pelletised biochars using Co Kα X-ray diffraction. See*

373   *Table 1 for sample nomenclature.*

Sample	Minerals detected
PAD450	SiO_2 $Na_2S_2O_3$ $K_{1.2}Al_4Si_8O_{20}(OH)_4.4H_2O$ $Na_3Mg_3Ca_5Al_{19}Si_{117}O_{272}$
PAD550	SiO_2 $Na_2S_2O_3$ $Na_{0.3}(AlMg)_2Si_4O_{10}(OH)_2.6H_2O$
EPAD450	SiO_2
EPAD550	SiO_2 $NaNO_3$
POCAD450	SiO_2 $Na_2S_2O_3$ MgS
POCAD550	SiO_2 $K_{1.2}Al_4Si_8O_{20}(OH)_4.4H_2O$
EPOCAD450	SiO_2 $Na_2S_2O_3$ $NaAl(SO_4)_2.11H_2O$ $Na_4Mn_5Si_{10}O_{24}(OH)_4.6H_2O$ $AlPO_4$
EPOCAD550	SiO_2

374

3.2 Surface characterisation of the pelletised biochars

3.2.1 X-ray photoelectron spectroscopy

377   XPS analysis was conducted on the exterior surfaces of POCAD450, POCAD550 and

378   EPOCAD450 pellets and the interior surfaces of a crushed pellet for POCAD450 and

379   EPOCAD450. A comparison of the C1s A, B, C and D; O1S A and B; and N1sA and B

380   bond states is depicted in Figure 1, and bonding mode designation is outlined in the

381   Supplementary Information.

382

Comparison of surface and whole sample XPS analyses of relative atomic % of bond states for POCAD450, POCAD550 and EPOCAD450
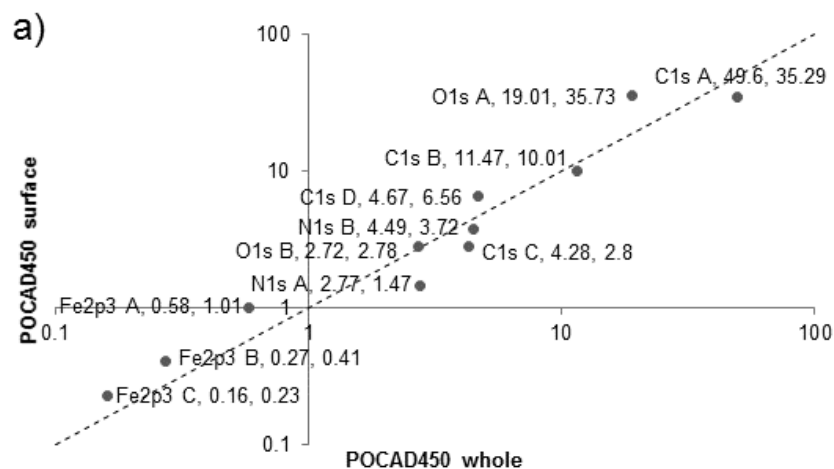

383
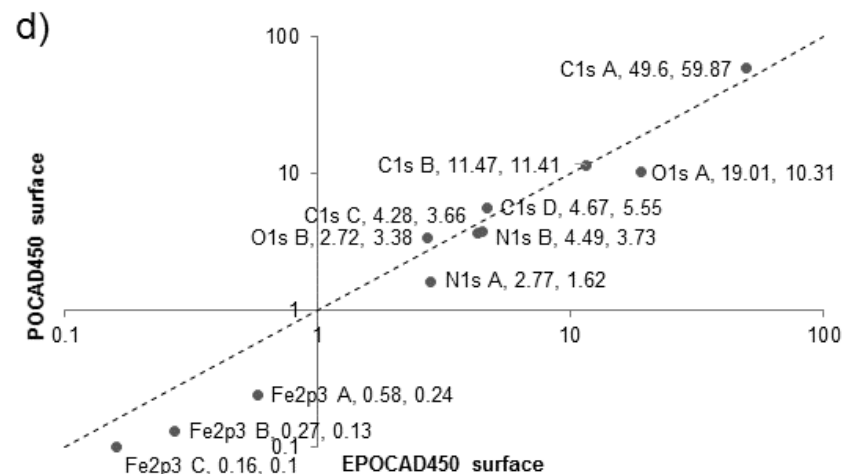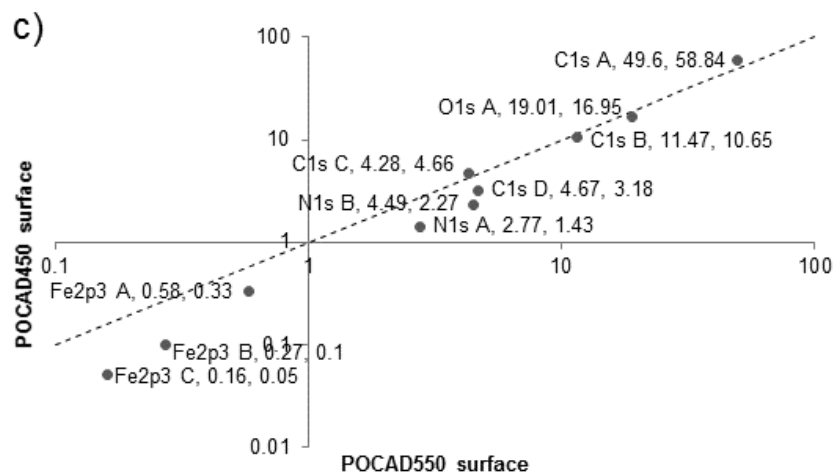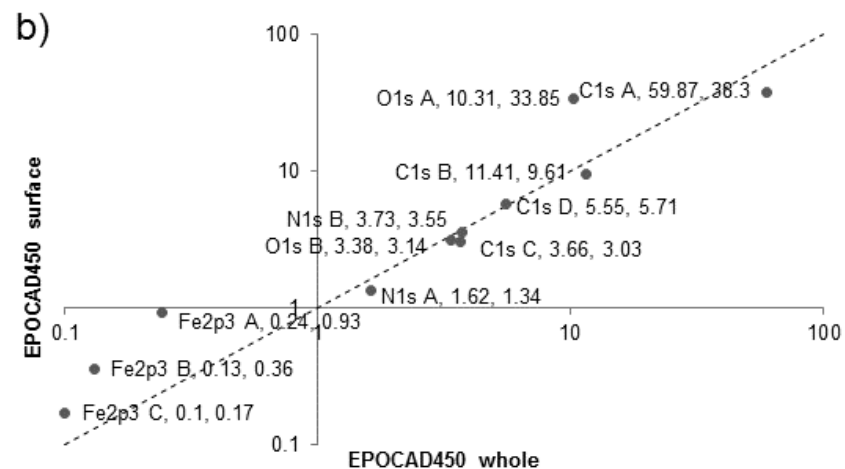
384   *Figure 1: Comparative log$_{10}$-log$_{10}$ plots of relative atomic percentage of bond states*

385   *identified by XPS. a) Comparison of POCAD450 surface and whole sample analyses. b)*

386   *Comparison of EPOCAD450 surface and whole sample analyses. c) Comparison of*

387   *POCAD450 and POCAD550 surface analyses. Bond state O1s B was detected for*

388   *POCAD450 (relative atomic precentage 2.72 %) but not POCAD550, so this does not*

389   *appear on the plot d) Comparison of POCAD450 and EPOCAD450 surface analyses.*

390

391   The Fe2p3 results for POCAD450 and EPOCAD450 (Supplementary Table 3a) did not

392   support the presence of Fe(0) or predominantly Fe(II) state iron compounds, as these

393   were not detectable. The binding energy spectra indicate the possible presence of the

394   Fe(III) compound Fe_2O_3 or FeOOH on the surface of POCAD450 with a peak at 710.85

395   eV, whilst the Fe2p3 A peak observed at 711.51 eV in the interior surface indicates the

396   presence of either the Fe(II)/(III) compound Fe_3O_4 and/or surface $Fe-O-PO_3^{2-}$. This

397   suggests that the overall concentration of Fe_2O_3 or FeOOH is relatively small compared

398   with the concentration of Fe_3O_4 and/or surface $Fe-O-PO_3^{2-}$. The surface of the

399   EPOCAD450 also produced a Fe2p3 peak at 711.56 eV rather than 710.85 eV. The

400   shifting of the Fe2p3 A peak from 710.85 eV and associated Fe^{3+} satellite peak at

401   718.65 eV on the surface of POCAD450 to 711.56 eV and 720.33 eV respectively in

402   EPOCAD450 may indicate $Fe-O-PO_3^{2-}$ bonding during P exposure, as phosphate-iron

403   interactions have been observed to cause similar energy shifts in previous studies

404   (Arshadi et al., 2015; Fang et al., 2015; Mallet et al., 2013). Both spectra indicate the

405   presence of iron sulfate compounds, which may be important.

406

407   The Fe2p3 peaks observed for the surface of POCAD550 differ slightly from those of

408   the 450°C pair. The Fe2p3 A peak, similar to the surface of EPOCAD450, is observed

409 at 711.52 eV, indicating either the presence of the Fe(II)/(III) compound Fe_3O_4 and/or

410 surface $Fe-O-PO_3^2$. The Fe2p3 B peak indicates the presence of $FeSO_4$, and/or is a

411 satellite of a Fe^{2+} peak. Importantly, the POCAD550 Fe2p3 C peak was uniquely

412 located at a lower energy of 708.82 eV, which indicates the presence of reduced Fe

413 compounds such as FeS_2, FeO and/or FeS.

414

415 Interpretation of the C, N, O and mineral peaks showed no differences in the proportion

416 of P, S, Ca, Fe and Na between POCAD450 and EPOCAD450 (Supplementary Table

417 3b). In terms of P, there is no difference in surface P concentration after P exposure as it

418 is very low relative to the native P concentration. The abundance of Si, C and N was

419 higher in relative terms for the EPOCAD450 pellet, while Al, O, F and Mg were

420 relatively less abundant. The only element present at a higher proportion on the surface

421 of EPOCAD450 compared to POCAD450 was C. In contrast to the whole sample

422 results, in the surface EPOCAD450 sample there was also lower detection of P, Si, Ca,

423 N, Fe, and Na compared to the surface of POCAD450.

424

425 Comparison of results for the surfaces of POCAD550 and POCAD450 pellets indicates

426 a higher proportion of C overall and lower proportions of P, S, N, O and Fe in

427 POCAD550. Heating of pure goethite (FeOOH) at temperatures > 600°C results in

428 sintering (Cornell and Schwertmann, 1996), so it is possible that the detection of a

429 lower proportion of Fe reflects sintering of Fe minerals at the 550°C HTT and a

430 decrease in overall Fe area, rather than loss of Fe from the biochar surface. The fact that

431 there was no difference in the distribution of the proportions of Al, Si, Ca and Mg

432 probably reflects the stability of minerals that contain these elements at higher

433 temperatures (Steenari and Lindqvist, 1998). At higher HTTs a higher proportion of C

434 relative to O may be expected, as O and H are more completely eliminated. It is possible

435 that proportionally more feedstock N, P and S was also eliminated in the preparation of

436 POCAD550 than POCAD450, on account of their own volatility (Magdziarz and Wilk,

437 2013).

438

439 **3.2.2 Laser ablation ICP-MS**

440 Mass spectral data from LA-ICP-MS analysis of POCAD450, POCAD550,

441 EPOCAD450 and EPOCAD550 were analysed to identify correlation of P with the

442 abundance of selected other elements: Al, Ca, Cu, Fe, K, Mg, Mn, Na, P, Pb, S and Si.

443 The selection of these elements was based on their predicted association with P and/or

444 their high concentrations within the biochars. The results are shown in Table 6, with

445 plots for the variation of elemental concentration per line scan in Supplementary

446 Figure 1. Phosphorus was significantly positively correlated with Mg, Al, K, Mn, Fe,

447 Cu and Pb for POCAD450, whilst after P exposure (EPOCAD450) the only strong

448 significant correlation ($\rho < 0.650$) was positive and was with Al. For POCAD550 there

449 was strong positive and significant correlation between P and Mg, Al, Si, K, Ca, Mn, Cu

450 and Pb. After P exposure (EPOCAD550), the correlations with Al, Si, K, Ca and Cu

451 remained highly significant. There was a marked difference between POCAD450 and

452 POCAD550 in the correlation coefficient of P with Fe (0.807 vs 0.462). For this reason,

453 correlations of Fe with other elements were also calculated (Table 6). Fe was strongly

454 and significantly positively correlated with P, Mg, S, Mn, Cu and Pb in POCAD450, but

455 only S and Mn in POCAD550. In EPOCAD550 the only significant correlation with Fe

456 that remained strong ($\rho < 0.650$) was with S, which was also positive.

457 *Table 6: Correlation coefficients of P and Fe to other elements analysed by LA-ICP-MS*

458 *(n = ~ 220). Spearman's ρ is reported, except for correlations marked with [P], where all*

459 *data were normally distributed so Pearson's product-moment correlation has been*

462

463

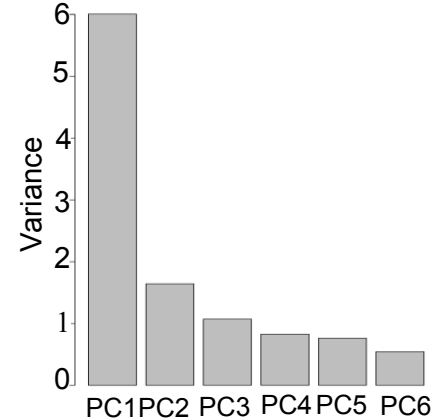|	POCAD450		EPOCAD450		POCAD550		EPOCAD550	
	P	Fe	P	Fe	P	Fe	P	Fe
Na	0.330****	0.160*	0.385****	N.S.	0.432****	0.324****	0.433****	N.S.
Mg	0.767****	0.679****	0.572****	0.348****	0.651****	0.419****	0.629****	N.S.
Al	0.789****	0.618****	0.665****	0.333****	0.772****	0.396****	0.818****	N.S.
Si	0.521****	0.397****	0.515****	0.202**	0.669$^{P, ****}$	0.453****	0.748****	N.S.
S	0.568****	0.866****	0.156*	0.342****	0.348$^{P, ****}$	0.857****	N.S.	0.838****
K	0.737****	0.601****	0.586****	0.209**	0.671****	0.373****	0.866****	N.S.
Ca	0.520****	0.446****	0.517****	0.286****	0.772****	0.480****	0.850****	N.S.
Mn	0.747****	0.861****	0.585****	0.788****	0.696****	0.888****	0.515****	0.628****
Fe	0.807****	-	0.484****	-	0.462****	-	N.S.	-
Cu	0.713****	0.688****	0.402****	0.467****	0.742****	0.497****	0.737****	N.S.
Pb	0.765****	0.697****	N.S.	0.270****	0.714$^{P, ****}$	0.530****	0.624****	N.S.

464 Principal Component Analysis (PCA) was also conducted on the LA-ICP-MS data to

465 identify the main clustering patterns of the elements on the surface of the biochars. The

466 PCA results are shown in Figure 2 and detailed information on the Principal

467 Components (PCs) of each sample is in Supplementary Tables S4–S7. Three PCs were

468 identified for POCAD450. The first PC axis separated sample locations from the line

469 scans (~220 for each biochar) enriched in Fe, Mn, S and Cu from sample locations

470 enriched in all other elements except for P, which was invariant along the second PC

471 axis. The concentration of all analysed elements increased along the second PC axis

472 apart from P. The clustering of elemental concentrations in the sample locations was

473 different after P exposure. Six PCs were identified for EPOCAD450. Along the first PC

474 axis, the concentrations of Al, Si, Ca, K, Na, Pb and S varied in the same direction,

475 whilst Mg, Cu, P, Mn and Fe concentrations varied together and separately from the

476 other group of elements. Again, the second PC axis separated sample locations which

477 contained either higher or lower concentrations of all of the analysed elements. Analysis

478 of the POCAD550 data revealed five PCs and similar sample locations distribution to

479 POCAD450 along the first PC, with a strong association between the concentrations of

480 Fe and S, the variance of which was also related to that of Mn. All other elemental

481 concentrations varied together, apart from Cu and Pb, which were invariant along the

482 second PC axis. Similar to EPOCAD450, quite different elemental sample location

483 distributions were identified after P exposure in EPOCAD550. Six PCs were identified,

484 with sample locations enriched in Na, Mg and Al separated from sample locations

485 enriched in Ca, Cu. Pb, Mn, Fe and S along the first PC axis. Iron and S were still

486 strongly covariant, whilst K, P and Si were invariant along the second PC axis. Along

487 the second PC axis, samples containing higher amounts of Fe and S separated from

488 samples enriched in all other elements analysed. Unlike the transition observed in

489 properties from POCAD450 to EPOCAD450, there was no evidence of dissociation of

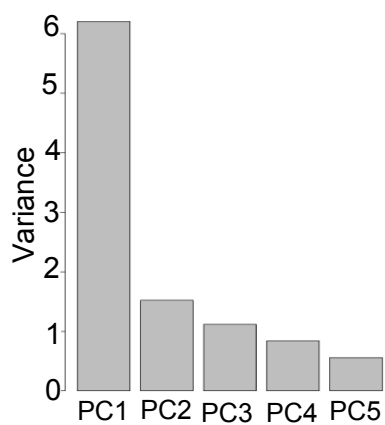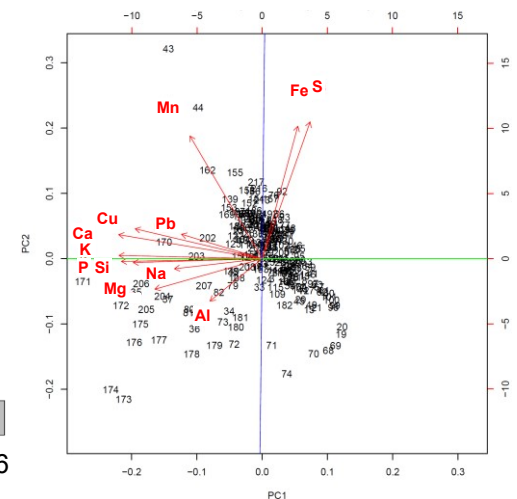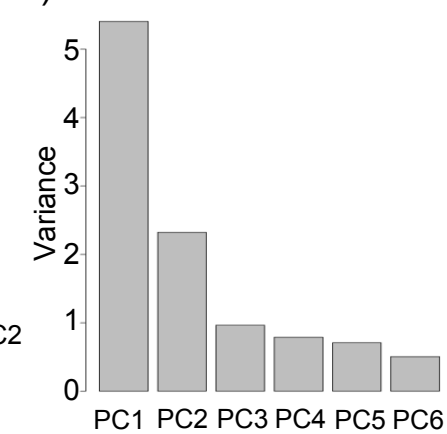490 Fe and S in the higher temperature POCAD550 biochar after P exposure.
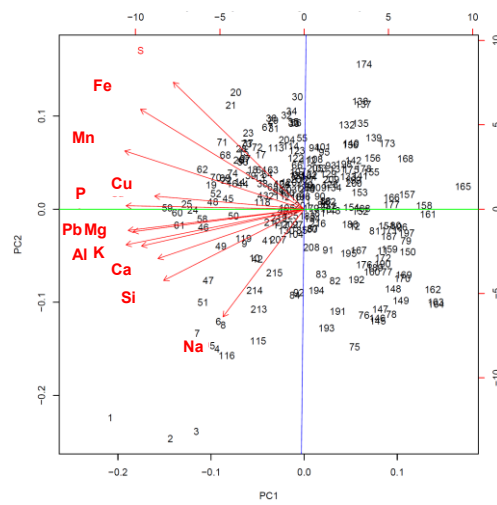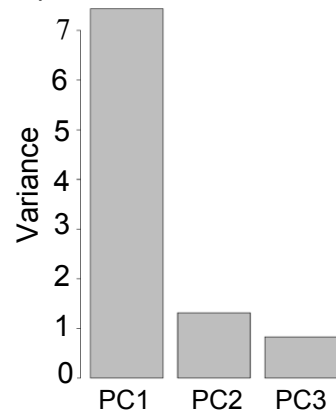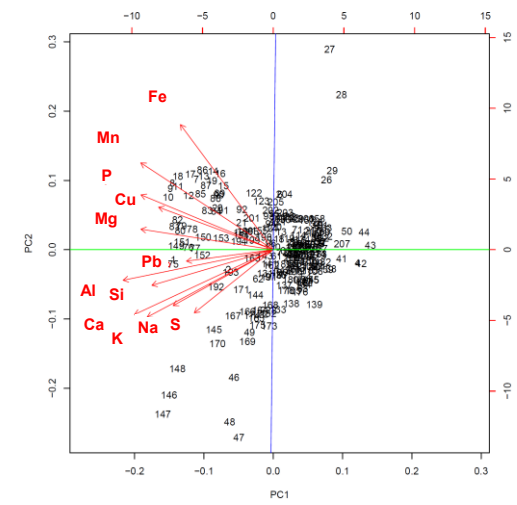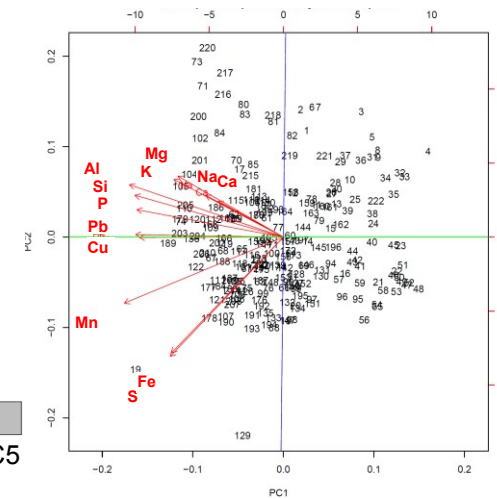
Figure 2: Principal component analysis of LA-ICP-MS spectral data obtained from a)

POCAD450 b) EPOCAD450 c) POCAD550 and d) EPOCAD550. For each analysis n

= ~220. The bar plots show proportion of variance of each principal component

identified in the analysis. The adjacent plots how the distribution of samples along the

first and second principal component axes, with arrows indicating the direction of the

relevant vectors.

3.2.3 Scanning electron microscopy with energy dispersive X-ray spectroscopy

Visual comparison of SEM-EDX images from PAD450 and EPAD450 (Figure 3a-b)

highlights the typical effect of P exposure on pores and mineral phases at the biochar

exterior surface. Although the EDX spectra show similar element proportions overall,

there is more P and Fe as well as considerably more exposed C (and somewhat less S)

in EPAD (Figure 3c-d).

SEM highlighted surface heterogeneity at various scales in the pelletised biochars

(Figure 4). Mineral phases in POCAD450 remain after P exposure (Figure 4a-1).

Carbon surfaces are revealed (Figure 4a-2) and distinctive crystalline mineral phases are

apparent (4a-3). The latter may have formed during the P exposure process or been

exposed by dissolution of other phases. The masking of a carbon framework by a

variety of Si-rich mineral phases is a feature commonly observed at high resolution

(Figure 4c). Phosphorus deposits may be observed in positions also relatively enriched

in Al, Ca and Fe (Figure 4f).

EDX mapping was used to visualise the co-location of elements in SEM images of

EPOCAD450 in a spot identified as carbon framework with mineral deposits (and

532   representative of other sites with similar morphology) (Figure 5). The map shows clear

533   separation of the carbon-rich area from other elements aside from O. The mineral

534   deposits were shown to contain predominantly P, Si, Al and O. EDX mapping of a spot

535   on POCAD550 (Figure 6) highlights the general elemental heterogeneity of the external

536   surfaces of the biochars observed during the SEM analyses. The maps show the location

537   of native P relative to other elements. Compared to EPOCAD550, a lower proportion of

538   C was measured at the surface of POCAD550. The same was observed for

539   EPOCAD450 compared to POCAD450. Aluminium, P, Fe and O were present across

540   the whole spot of POCAD550 mapped in Figure 6, but were also concentrated in small

541   1–10 μm domains. Calcium was found to be located diffusely across the right side of the

542   image, but only in concentrated domains to the left. Sulfur, Si and Mg were

543   predominantly found in concentrated phases. The relative distribution of P, C, Ca, Si, Al

544   and Fe can be seen in the overlay maps at the bottom of Figure 6, which supports the

545   findings of Ca, Si and Al co-variation and Fe and P covariation in the LA-ICP-MS

546   analysis of POCAD550 in Figure 2. Additional structural and chemical detail can be

547   found in additional SEM images, EDX spectra and maps in Supplementary Figures S2-
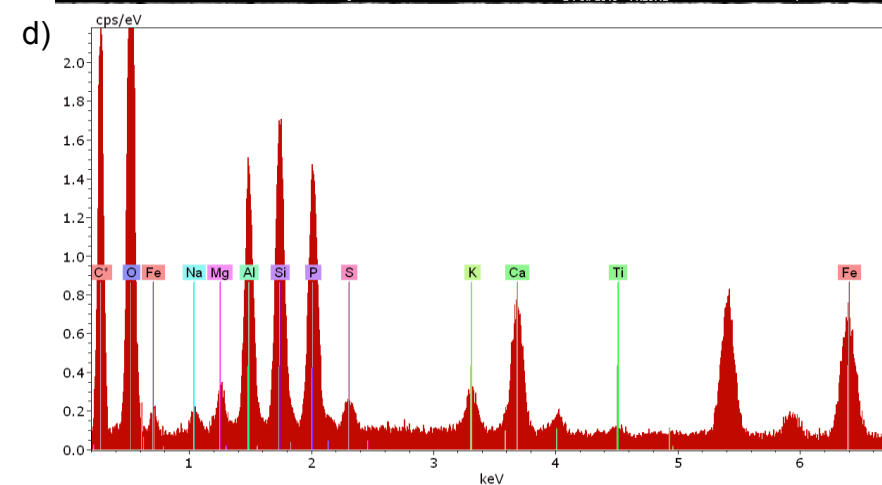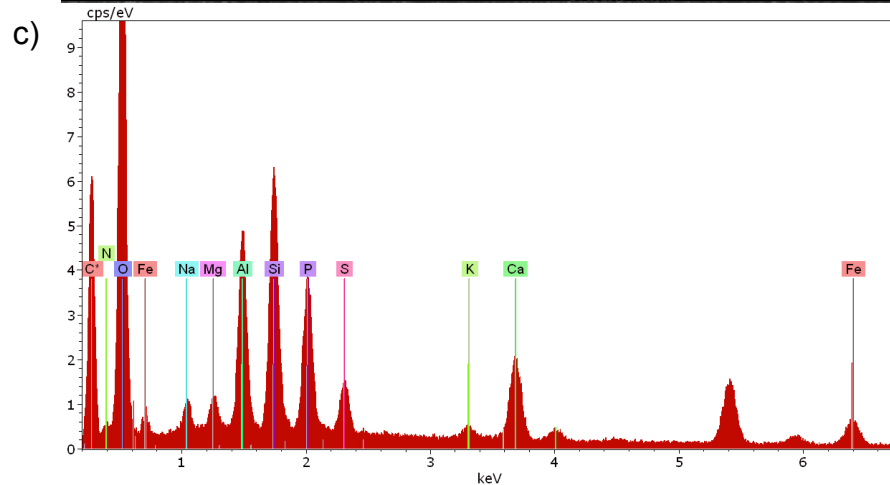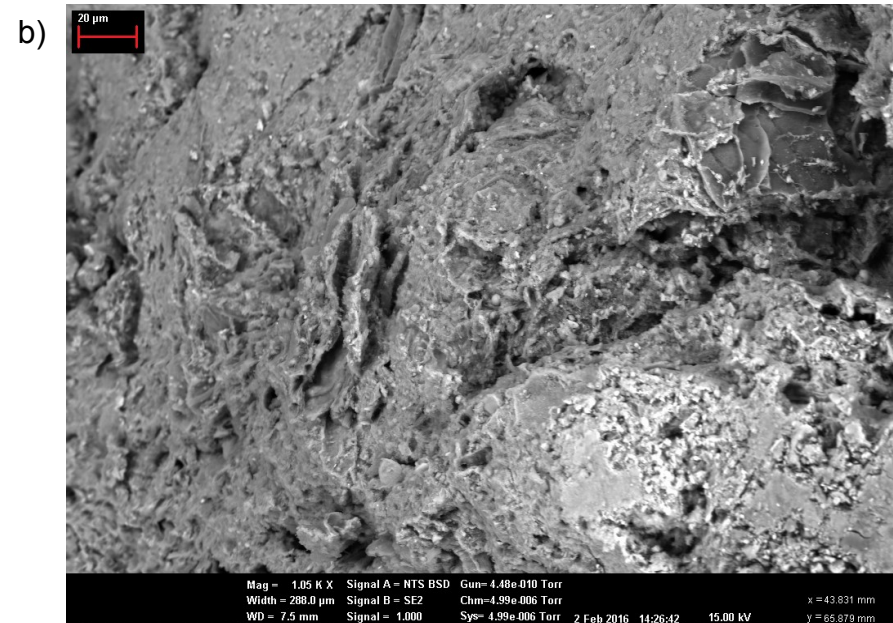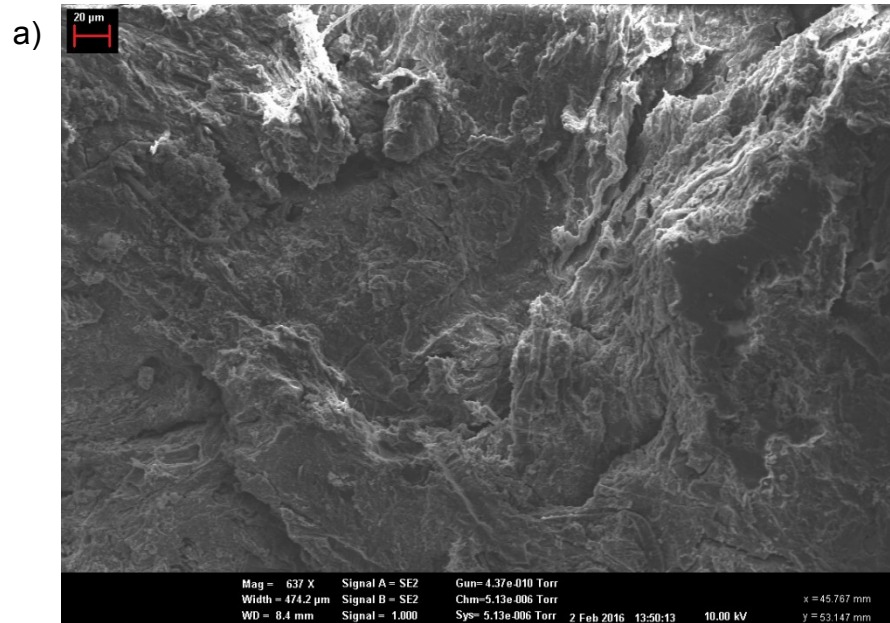
548   S6.

Figure 3: SEM and EDX spectrum of PAD450 (a,c) and EPAD450 (b,d) showing differences in surface morphology pre (PAD450) and post (EPAD450) P exposure.
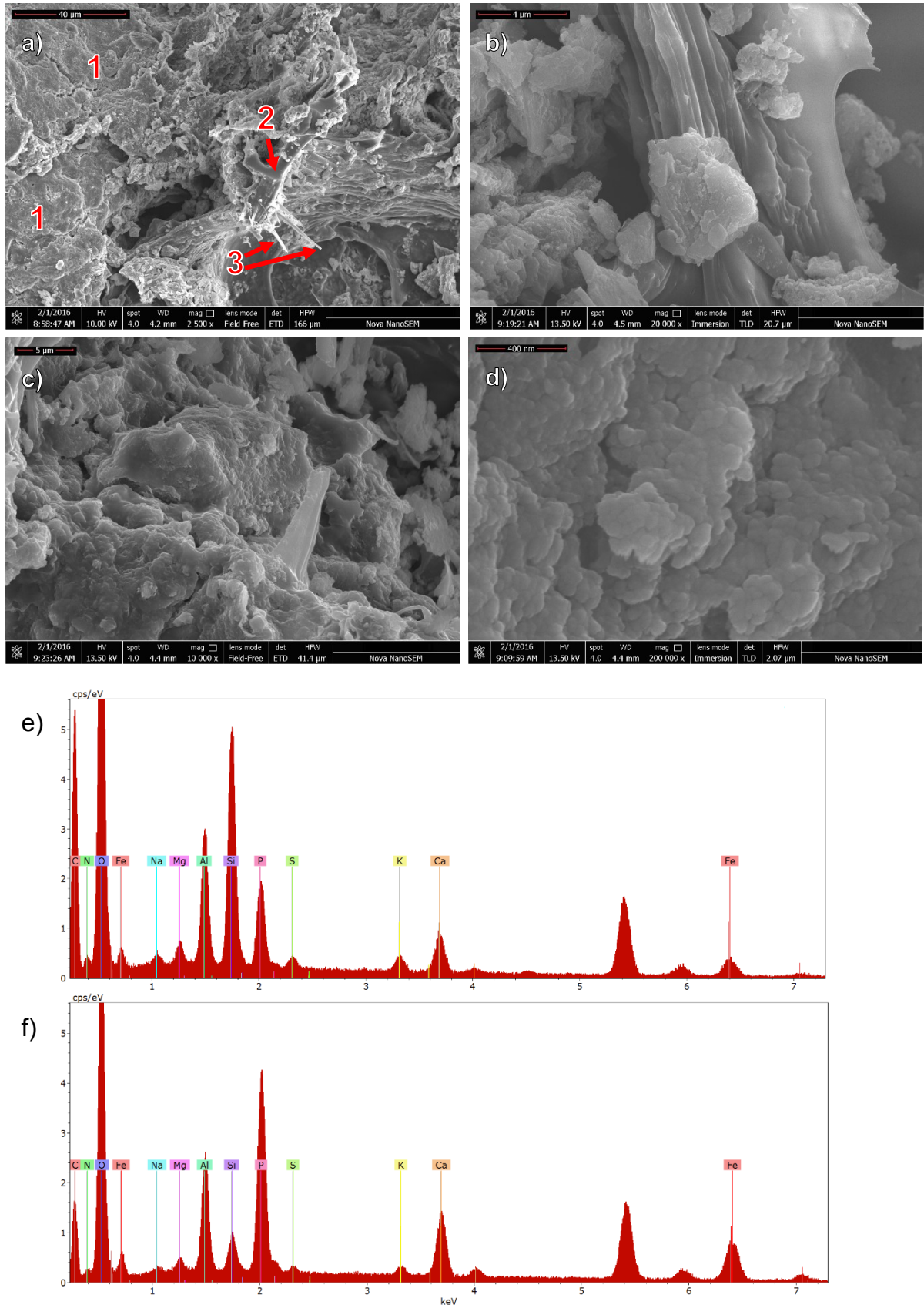
Figure 4: SEM-EDX data obtained from EPOCAD450. SEM image a) shows clay

mineral phases (1), exposed carbon lattice (2) and newly formed or exposed mineral

phases (3). SEM image b) shows mineral particles around the carbon lattice. Image c)

shows the heterogeneous nature of the surface, and EDX spectrum d) shows the

elements present in c), e) shows high magnification SEM image and EDX spectra of P

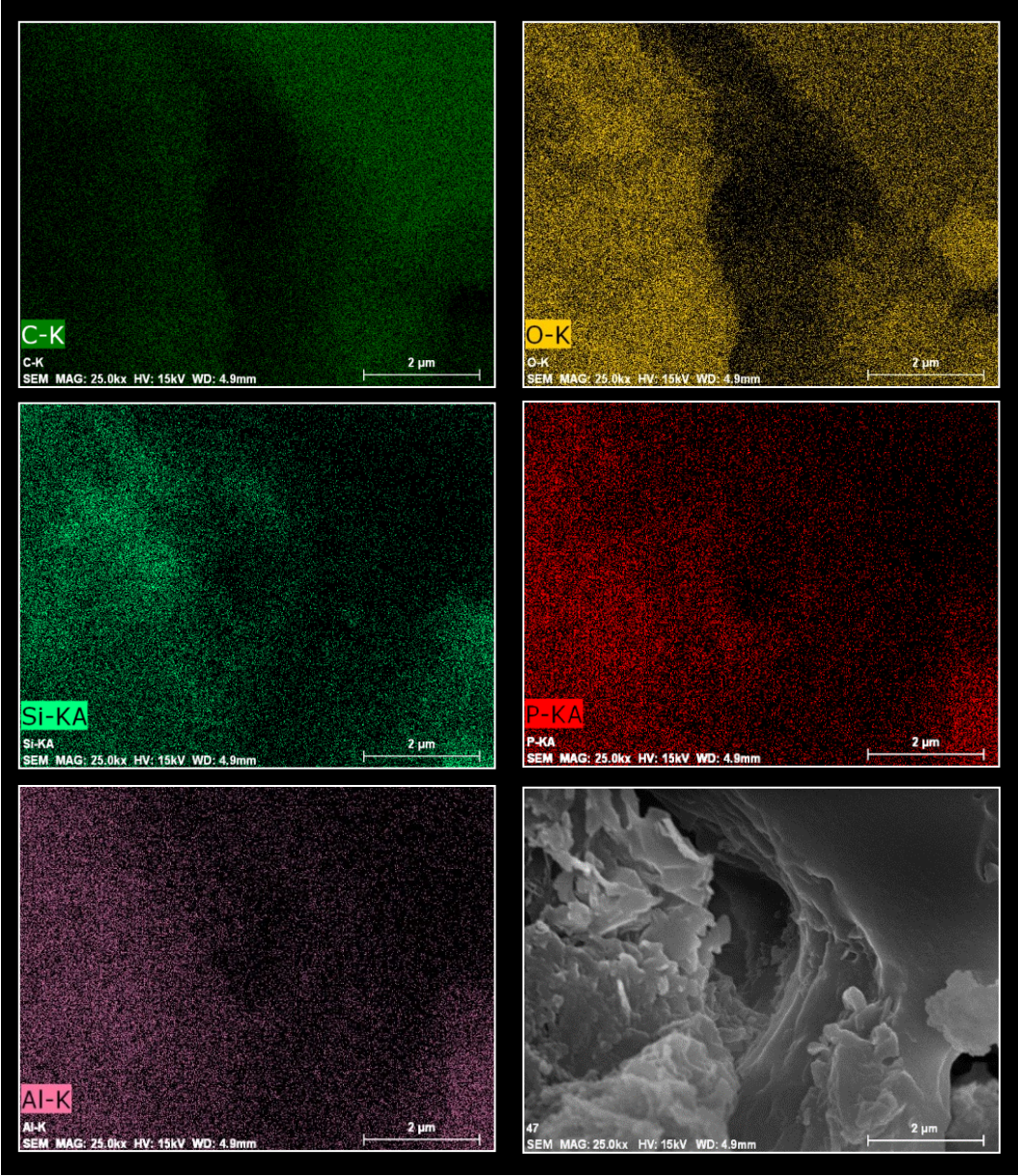*deposits on the surface of EPOCAD and f) shows the elements present in e).*

Figure 5: SEM-EDX map of EPOCAD450, showing spatial separation of C with O, Si,
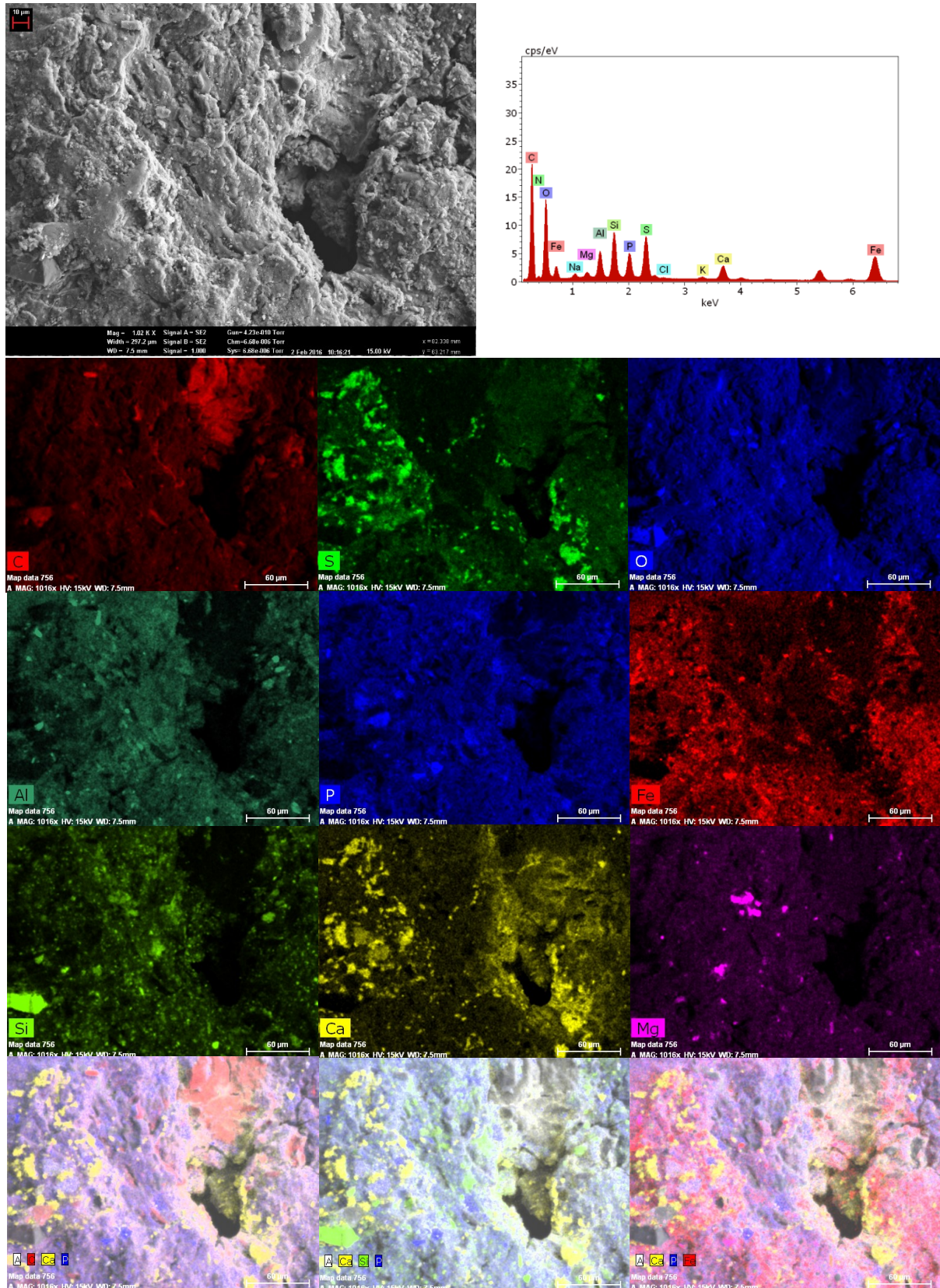
P and Al.

Figure 6: SEM-EDX map of POCAD550, showing the localisation of native P (centre), as well as C, S, O, Al, Fe, Si, Ca, and Mg. Overlay maps of C (red), Ca (yellow) and P (blue); Ca (yellow), Si (green) and P (blue); and Ca (yellow), P (blue) and Fe (red) are also shown.

4. Discussion

4.1 Effect of feedstock composition, processing and pyrolysis conditions on P capture

The results of this study demonstrate that the interaction of P (as phosphate) with sewage sludge-derived biochar is not a simple process which can be described by one specific mechanism or element within the biochar matrix. At the macroscale (i.e. the particle scale – mg and mm), each specific sewage sludge/ochre biochar material is quite homogeneous, as demonstrated by the low standard deviations of replicated determinations of total element composition by ICP-OES analyses of sample digests (Tables 2 and 3) and of P uptake in the experiments with more uniform material sizes (Shepherd et al., 2016). This reflects sufficient feedstock blending and indicates that the pyrolysis process has occurred uniformly throughout the materials. In contrast, the results of the XRD, SEM and LA-ICP-MS analyses highlight the microscale heterogeneity of the materials. Although microscale heterogeneity is not necessarily important for overall P capture capacity, more detailed studies of biochar microscale structure in future work would provide better insights into mineralogy, which may further assist in the selection of optimal HTT and feedstock blends for P capture and release, especially when mineral wastes of variable composition are used as the source of P-reactive elements.

4.1.1 Iron plays a key role in P capture for biochars produced at 450°C

Relatively small additions of ochre (10 % w/w) in the feedstock increased the Fe concentration in pelletised POCAD biochars by 54–61% compared to the sewage sludge-only equivalents (PAD). This is important, as Fe was the only element found to

33

641   be strongly and significantly correlated positively to P uptake after 5 days exposure to

642   P.

643

644   Considering the findings of Sibrell et al. (2009) examining P capture in ochres with

645   differing chemical compositions, it is possible that the superior P capture characteristics

646   demonstrated by AD450 could be related to the relatively equal content of Al and Fe in

647   AD450 compared to AD550 (1:1.12 vs 1:1.6). Although the ochre-containing biochars

648   captured more P from 5 days repeated exposure to a 20 mg l^{-1} solution, the mean P

649   capture by AD450 was slightly higher (though not significantly) than that of OCAD450

650   from both the 800 mg l^{-1} P (9.72 ± 0.657 mg P g^{-1} compared to 9.37 ± 0.872 mg P l^{-1})

651   and the 3 g l^{-1} P solutions (25.9 ± 5.10 mg P g^{-1} compared to 20.4 ± 6.35 mg P g^{-1}). This

652   indicates that, although a greater concentration of Fe may increase the rate of P capture

653   at low concentrations of external P solution, a balance of Al and Fe may favour the

654   reaction kinetics for P removal at higher external P concentration.(Ainsworth et al.,

655   1985) This is an important consideration for feedstock design, as mineral waste rich in

656   Al may be more suitable for combination with Fe-rich sewage sludge than iron ochre

657   for applications targeted at capturing P from high concentration P sources, but only if

658   they are to be used in non-acidic soils, or in conjunction with liming treatments to

659   mitigate Al toxicity to plants. Al was strongly and significantly correlated with P before

660   and after P exposure in the LA-ICP-MS analyses, further indicating the importance of

661   Al for P capture by biochar.

662

663   **4.1.2 Feedstock pelletisation affects elemental composition of biochar**

664   Comparison of the newly prepared pelletised biochars and non-pelletised biochars

665   previously described in Shepherd et al. (2016) showed that pelletisation and/or

continuous (rather than batch) pyrolysis processing results in greater overall retention of

elements within the biochar matrix, relative to carbon. This is most likely due to a

reduction in the loss of material to the gas phase, or a different trajectory of pyrolytic

reactions in the continuous-flow furnace compared to the gradual heating process in a

batch kiln. Rapid expulsion of gases from the pellets as the cold feedstock reaches the

hot continuous-flow kiln may result in different pyrolytic reactions than if the feedstock

was slowly heated to the same temperature, similar to the reported explanation for the

differences between gas, oil and solid yield between fast and slow pyrolysis (Onay and

Kockar, 2003).

4.1.3 Increasing highest treatment temperature changes iron oxidation state, sulfur interactions and mineral structure

Comparison of elemental variation in the first PC in the analysis of LA-ICP-MS results

shows great similarity between POCAD450 and POCAD550, accounting for 77 and

61% of sample variance respectively. Covariance of Fe, S and Mn was identified in

both, however the correlation of Fe and S was much stronger in POCAD550 than

POCAD450 (Figure 2), indicating possible differences in mineral structure due to

pyrolysis HTT.

The stronger relationship between Fe and S in POCAD550 compared to POCAD450

was supported by visual evidence from SEM-EDX. EDX analyses of POCAD450

revealed sites where Fe and S were covariant (as in Supplementary Figure S4a), and

non-covariant (as in Supplementary Figures S4b-c and S5), whilst the same analysis of

POCAD550 revealed more sites where Fe and S were found in higher concentrations

together (Figure 6 and Supplementary Figure S7). These results may suggest reduced

691   iron species (Fe(I) or Fe(II)) are present in POCAD550, but not POCAD450 or

692   EPOCAD450, where Fe appears to be present in Fe(III) and mixed Fe(II/III)

693   compounds.

694

695   Considering these points together, is possible that at the 550°C HTT insoluble, reduced

696   Fe/S compounds have formed to a greater extent than at 450°C, in addition to complex

697   mixed mineral phases that contain both Fe and S. Further high-resolution analysis using

698   Thermogravimetric analysis–mass spectroscopy (TG-MS), soft X-rays and

699   Transmission electron microscopy (TEM) would be required to clarify this.

700

701   The ochre used in this study consisted of 100% goethite (Carr, 2012). When heated to

702   temperatures between 140–500°C in the presence of air, goethite transforms to

703   haematite by thermal dihydroxylation (Cornell and Schwertmann, 1996). Under

704   reducing pyrolysis conditions and the presence of carbon, it is also possible that

705   magnetite (Fe_3O_4, Fe (II)(III) oxide) and maghemite (γFe_2O_3, Fe(III) oxide) forms

706   (Campbell et al., 1997). Thermal treatment of goethite results in the development of

707   microporosity due to expulsion of water from the mineral lattice, creating more surfaces

708   with which P can react. Pore sizes increase further as temperatures increase, however, as

709   previously discussed, above 600°C the mineral sinters, which results in a large decrease

710   in porosity (Cornell and Schwertmann, 1996). Hence pyrolysis HTTs of less than 600°C

711   may be necessary for biochars containing large amounts of iron oxyhydroxides if high

712   surface area and P reactivity are desired.

713

714   **4.2 P capture processes**

715   **4.2.1 The role of organic functional groups on biochar surfaces in P capture**

716   Despite the modest pyrolysis temperatures used in this study, SEM-EDX mapping and

717   XPS analysis did not provide strong evidence for C-O-P bonding, or carbon

718   functionality generally. It has been suggested that phosphate could undergo ligand

719   exchange with hydroxyl or carboxyl groups on the surface of the biochar carbon lattice

720   (Laird and Rogovska, 2015), however ligand exchange reactions only occur in metal

721   complexes. Synthesis of the proposed phosphoester species proceeds via a condensation

722   reaction, is favoured by decreasing pH (inconsistent with biochar surfaces), and requires

723   high temperatures, condensing agents or condensed phosphate reagents, which also

724   require significant temperatures for synthesis (Gull et al., 2014). In biological systems

725   (at pH values closer to 7) the phosphorylation reaction requires enzyme catalysis, so the

726   proposed mechanisms are unlikely to occur on biochar surfaces in environmental

727   systems unless mediated by an organism which has some biological need to perform

728   this reaction.

729

730   There is no evidence, in this study or in the literature, to suggest that the carbon fraction

731   of biochar plays a major role in P capture, other than providing an essential support on

732   which the mineral elements which do interact with P can be anchored, and improving

733   the value of the end-product for use in agriculture. A significant increase in P sorption

734   was observed in washed compared to unwashed oak biochar (Hollister et al., 2013),

735   however the concentration of P sorbed by even the washed biochar was quite small

736   (0.077 mg P g^{-1}, 13.5% of the lowest amount of P captured in this study), so the effect

737   of washing to expose carbon surfaces appears to be over-estimated. The increasingly

738   common practice of adding chemical elements to biochar for P capture enhancement is

739   additional evidence for this assertion (Chen et al., 2011; Fang et al., 2015; Li et al.,

740   2016; Park et al., 2015; Ren et al., 2015; Yao et al., 2011; Zhang et al., 2013, 2012). It is

741 evident that metal cation-mediated interactions with organic functional groups on

742 biochar surfaces (or precipitation reactions) explain the high P capture capacities

743 demonstrated by particular biochars.

744

745 The point of zero charge (PZC) of biochars reported in the literature are generally low

746 (Mukherjee et al., 2011; Qiu et al., 2009; Silber et al., 2010), so it is likely that at pH > 3

747 biochar surfaces will be negatively charged. Theoretically, at high pH a hydroxyl or

748 carboxyl group on the surface of biochar will be deprotonated in solution, forming an

749 oxyanion which will be resonance stabilised by the delocalisation of electrons in the

750 aromatic biochar structure. This makes these groups more acidic than the equivalent

751 group in an aryl alcohol. The oxyanion will be nucleophilic, and could attack the

752 phosphate P (capturing the phosphate from solution), which, under basic conditions,

753 will be relatively electron poor due to the presence of two electronegative oxyanions

754 and a C=O group. The likelihood of these two negatively charged species coming

755 together for reaction is low, however, due to electrostatic repulsion. Cations in solution

756 may reduce this effect but, even so, the nucleophilic attack of the phosphate P by the

757 biochar oxyanion is also sterically hindered. The equivalent argument can be made for

758 the potential interactions between phosphate and N-heterocycles on biochar surfaces.

759 Whilst not chemically impossible, the likelihood is low of these reactions contributing

760 in any significant way to P capture mechanisms in biochar materials in wastewater

761 treatment systems.

762

763 **4.3 Conceptual model of P capture by biochar from aqueous solution**

764 **4.3.1 Initial solubilisation and mobilisation of native biochar components**

765 In the P capture experiments biochar is held in aqueous P solution buffered at pH 7. A

766 simplified reaction mechanism for the interaction of aqueous phosphate with metal

767 oxides on the biochar surface is given in Figure 7. Soluble organic and mineral

768 compounds are presumably released into solution at a rate that depends on their

769 proximity to the surface of the biochar (limited by pore size and connectivity) as well as

770 their solubility in the P solution and binding mechanisms. As demonstrated for soil, the

771 energy required for P exchange from soil water to soil particles is very similar to that of

772 the reverse reaction (Barrow, 2015), so the direction of this reaction in biochar (i.e. P

773 capture or release) will be similarly dictated partly by the amount of P already within

774 the biochar structure relative to its capacity for P uptake (probably related to the

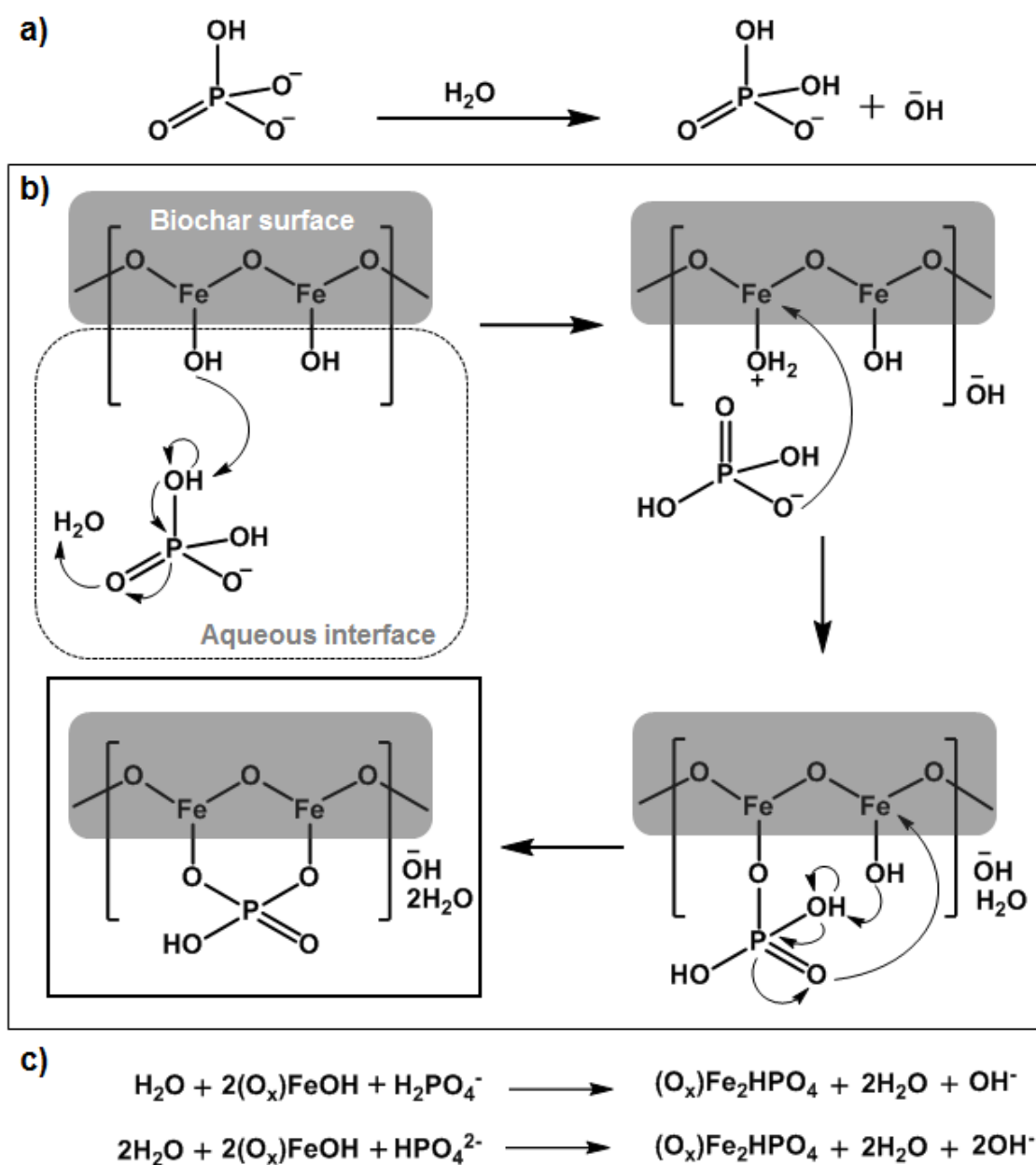775 concentration and composition of certain mineral components).

Figure 7: Likely predominant AD sewage sludge biochar P sorption mechanism where

the metal = $M^{2+/3+}$. Iron oxyhydroxides are presented based on the experimental

evidence pointing to their significance in these biochars. (a) In a pH 7 buffered aqueous

environment the basic phosphate species HPO_4^{2-} reacts with water to form the acidic

$H_2PO_4^-$ species. (b) Deprotonation of a phosphate hydroxide moiety by the iron

oxyhydroxide, followed by phosphate rearrangement and subsequent deprotonation of a

water molecule, producing hydroxide, regenerates $H_2PO_4^-$ and renders the iron prone

to nucleophilic attack by phosphate. The process can repeat on an adjacent

785 *ironoxyhydroxide moiety, forming a stabilised ring structure. (c) Balanced equations*

786 *for the overall reaction where either $H_2PO_4^-$ or HPO_4^{2-} is the starting species.*

787

788 The initial process of solubilisation of different phases within the biochar structure is

789 likely to open up the pore structure, as evident in Figures 2–4 and Supplementary

790 Figures S2–S6. It is possible that, due to the comparatively low ratio of C compared to

791 minerals in the sewage sludge feedstock, the carbon structure will contain a range of

792 pore sizes. Physical determinations of porosity were not undertaken in this study, but

793 visual SEM observation supports this hypothesis. During pyrolysis non-volatile mineral

794 elements are likely to restrict the formation of aromatic sheets and promote pore

795 formation (Rawal et al., 2016).

796

797 XPS analysis of surface and whole samples of POCAD450 and EPOCAD450 revealed a

798 "loss" of P, Si, Ca, N, Fe, and Na from the exterior (but not interior) surfaces after P

799 exposure. It is possible that this reflects solubilisation and loss of these elements from

800 the surface into solution during P exposure, but another explanation is that the elements

801 were re-arranged on the surface after initial solubilisation, forming localised mineral

802 complexes (Figures 8 and 9). The formation of these complexes would result in

803 exposure of the carbon lattice, as seen in the SEM images (Figures 2–4), coupled with

804 mineral expansion out from (rather than laterally across) exterior surfaces. In XPS

805 analysis after P exposure mineral elements located closer to the biochar surface might

806 not be detected owing to masking by mineral layers and thus falsely appear to been

807 "lost". The LA-ICP-MS results also indicate that solubilisation and re-association

808 occurred, with the number of significant correlations between P and other elements

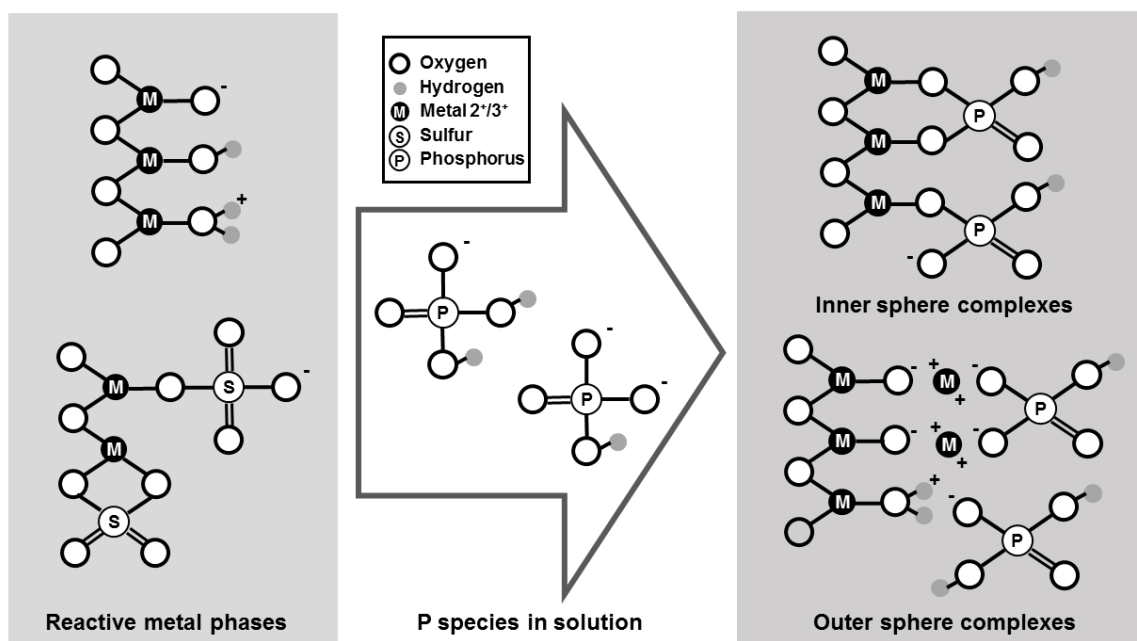809 lower in EPOCAD than corresponding POCAD biochars.

810

Figure 8: Phosphate-reactive metal phases on the biochar surfaces in these biochars.

811

The degree of hydrogenation of the metal oxides decreases with increasing pH and is

812

affected by the pyrolysis highest treatment temperature (HTT). Experimental

813

observations indicate that in addition to hydroxyl ligand exchange, biochar phosphate

814

capture also occurs at sites vacated by sulfate. These reactive sites can form inner

815

sphere and outer sphere compounds with phosphate, with some examples shown.

816

817

The SEM-EDX, LA-ICP-MS and XRD analyses collectively suggest that non-soluble

818

mineral phases remain on and in the biochar structure after P exposure. If this is correct,

819

non-soluble phases anchored on biochar surfaces via soluble organic or mineral phases

820

would become detached from the surface over time, as other phases dissolve. Minerals

821

on the external surface of the biochar would then be lost from biochar into solution,

822

those remaining in pores either being washed out over time or remaining trapped.

823

Surface area to volume ratio and pore structure may affect the release of less soluble
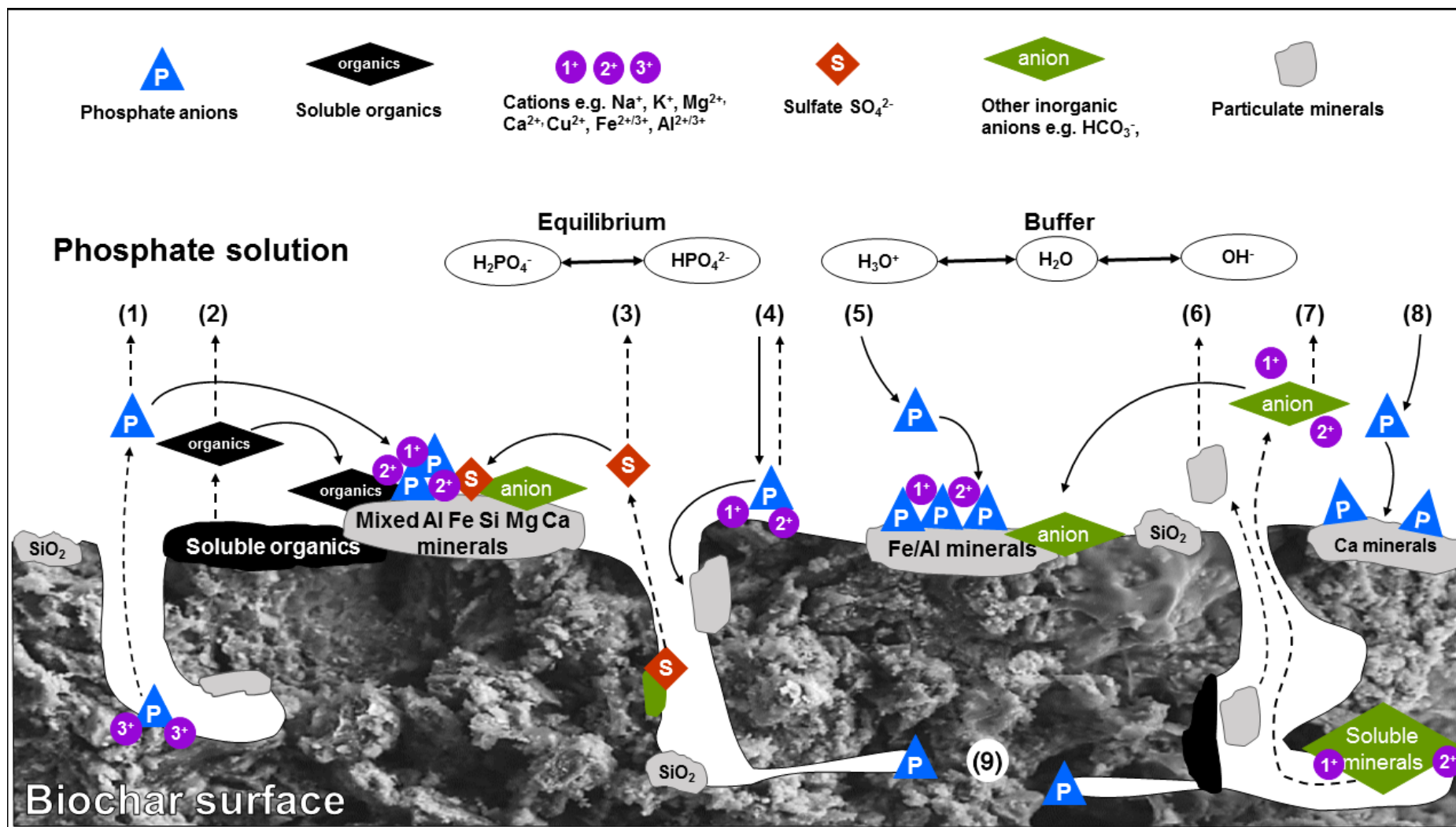
824

mineral phases.

825

Figure 9: Graphical representation of reactions which occur when biochar is placed in a pH 7 buffered phosphate solution. (1) Dissolution of phosphate from soluble ash/mineral phases. Phosphate may be released into solution or re-associate with biochar surfaces via mineral or organomineral interactions with other mixed species, such as Al, Fe, Si, Mg, Ca, K and Na in these materials. (2) Dissolution of soluble organic species from surfaces. These species may stay in solution or re-associate with species on the surfaces in organomineral clusters. (3) Dissolution of sulfate minerals (as observed in the biochars produced at 450°C). Sulfate may stay in solution or re-associate with surfaces in mineral or organomineral clusters. (4) Electrostatic association of phosphate to biochar surfaces via cation mediated interactions with surface organic functional groups. Phosphate may either be re-released into solution due to the relative weakness of the interactions or react chemically with mineral phases resulting in stronger retention. (5) Chemisorption of phosphate to iron and/or aluminium oxide phases on the biochar surfaces. (6) Release of insoluble ash and mineral phases into the aqueous phase due to weak binding or lack of binding to biochar surfaces. (7) Solubilisation of other minerals from within the biochar structure. (8) Precipitation of phosphates from solution with calcium mineral phases. (9) Native phosphate phases will be found within the biochar pore structure and will not be immediately accessible for dissolution, as per scenario (1). These phases will be released more gradually, over time.

4.3.2 Interaction of P with biochar surfaces and mobilised elements

In a solution phosphate interacts with solubilised mineral elements to form phosphate complexes which, depending on the phosphate coordination mechanism, can also interact with soluble organic compounds or organic surface-bound functional groups.

852   Once chemically bound or precipitated onto a surface phosphate-mineral and -

853   organomineral compounds can interact with other elements in solution. Phosphate

854   ligands can be labile and coordinate to metals in different ways, e.g. monodentate vs

855   bidentate coordination via O atoms (Arai and Sparks, 2001). Thus the way in which

856   phosphate binds to the surface of biochar is dependent on the other species present and

857   will change over time as different compounds dissolve and the local environment

858   changes (see Figures 8 and 9).

859

860   **4.3.2.1 Monovalent cations interrupt P capture and enhances P release**

861   For the 20 mg l^{-1} P treatments (Shepherd et al., 2016), Al, Cu, K, Na, and Zn

862   concentrations in the biochars were all significantly negatively correlated with P capture

863   on day 1. In addition, Pb was negatively correlated with P capture on day 5 (Table 4).

864   The presence of high concentrations of mono- and divalent salts in the biochar samples

865   that could dissolve in the P exposure experiments (Tables 2 and 3) may result in

866   stabilisation of the $H_2PO_4^-$ anion in solution, reducing the rate of capture. Furthermore,

867   K from the K_2HPO_4 used to make the phosphate solution would exacerbate this effect.

868   Indeed the lack of similar correlations in the day 5 and 800 mg P l^{-1} treatments supports

869   this interpretation, as by day 5 much of the K and Na will have leached from the biochar

870   and, in the higher concentration experiments the concentration of phosphate will be

871   much higher relative to the concentrations of K and Na leaching from the biochar.

872   Positive correlation of Na with P release also supports this interpretation.

873

874   In the 800 mg l^{-1} P experiments and not the 20 mg l^{-1} P experiments, however, K is

875   negatively (but not significantly) associated with P release (Pearson's product-moment

876   correlation = -0.636, p value = 0.175). This may be an electrostatic effect, where excess

877 K from the higher concentration treatment (added with the phosphate solution as

878 K_2HPO_4) interacts with the biochar surface making it more positively charged, reducing

879 the repulsion effect that slows down P capture over time (Barrow, 2015). As ash is

880 washed from the biochar during the experiment, more of the negative carbon functional

881 groups of the biochar are exposed, increasing the possibility for K to interact in this

882 way. For the higher concentration treatments at least, any effect of K on P capture and

883 release is most likely an artefact of the experimental setup and may not be observed

884 when the materials are used in a wastewater treatment plant.

885

886 **4.3.2.2 Mixed Fe and Al minerals are involved in P capture**

887 Biochar Fe concentration was significantly positively correlated with P capture and

888 negatively correlated with P release. As well as P captured during the adsorption

889 experiments, XPS analysis indicated that native P is associated with Fe in the biochars.

890 Phosphorus and Fe can react during pyrolysis, especially when ochre is present in the

891 feedstock as during pyrolysis as it can act as an acid catalyst (Joseph et al., 2013). Clay,

892 when heated, can liberate a range of chemical species including HF, HC1, HBr, H_2S and

893 HP (Heller-Kallai et al., 1988). Interior biochar surfaces characterised by XPS showed

894 the presence of Fe_3O_4 in both POCAD450 and EPOCAD450 as well as the surface of

895 the latter, whilst Fe_2O_3 was only identified on the surface of POCAD450. It is possible

896 that P exposure acts to prevent oxidation of the biochar surfaces, and that P sorption

897 occurs without oxidising Fe(II), therefore possibly only occurring at Fe(III) sites, but

898 additional XPS analysis would be required to fully explore these hypotheses.

899

900 For pelletised biochar from sludge–ochre mixes correlation analysis using LA-ICP-MS

901 data showed strongly significant positive correlation between the concentration of P and

902   Al after P exposure (EPOCAD450) or with Al, Si, K, Ca and Cu (EPOCAD550). PCA

903   of LA-ICP-MS data for the P-exposed EPOCAD450 biochar showed that P

904   concentration variation was related to that of Fe, Mn, Cu and Mg in the first and second

905   PCs. Compared to POCAD450, the relationship between the variance of Fe and Mn

906   with P was stronger whilst the relationship of P with the variance of S decreased,

907   suggesting replacement of sulfate by phosphate as a potential sorption mechanism,

908   which is supported by the SEM-EDX data. This was not the case for EPOCAD550, in

909   which P concentration variation was not related to that of Fe, S and Mn in the first and

910   second PCs, yet the relationship between the variance of Fe and S in POCAD550 was

911   maintained after P exposure, suggesting a different mechanism of P capture compared

912   to POCAD450. The bulk P capture for POCAD450 and POCAD550 were nearly

913   identical (0.95 ± 0.18 mg P g^{-1} and 0.95 ± 0.23 mg P g^{-1}, respectively), so although it

914   appears that different mechanisms predominate in biochars prepared at contrasting

915   HTTs, the net effect on P capture is similar. The heterogeneity of the biochars and

916   therefore P capture mechanisms most likely increases, as evidenced by the increased

917   number of PCs in the EPOCAD compared to POCAD biochars, as well as the smaller

918   relative contribution of PC1 in the former cases. These analyses provide information on

919   the main sources of variation between sample locations on the biochar surface but also

920   highlight the high amount of heterogeneity on the microscale.

921

922   Although Ca was only identified as strongly significantly correlated to P capture in the

923   LA-ICP-MS analysis of EPOCAD550, as it is present at a relatively high abundance in

924   the biochars it is likely that precipitation of P by Ca occurs in each of them to some

925   extent. The buffered pH 7 of the system may not favour this reaction, which could

926   explain why Ca concentration did not correlate with P capture consistently. High P

927   capture from mallee tree biochar produced at 720°C HTT has been reported in the

928   literature (Zhang et al., 2016). The authors suggest that the mechanism of P capture is

929   via precipitation of P as $CaHPO_4$ by substituting for HCO_3^{2+} and OH^- on $CaHCO_3^+$ or

930     $Ca(OH)_2$ mineral surfaces of the biochar. This seems quite likely, as the biochar had a

931   pH of 10.2, which strongly favours Ca phosphate precipitation, and contained 1.3% Ca

932   by weight but no Fe or Al. Importantly, whilst washing of the biochar with deionised

933   water significantly increased P capture but did not greatly affect Ca concentration,

934   washing with acid significantly decreased P capture, with an associated decrease of Ca

935   content in the biochar to 0.1%. The precipitation of hydroxyapatite was observed in

936   similar experiments obtained using cement-bound ochre to capture P from a non-

937   buffered P solution (Littler et al., 2013).

938

939   **4.4 Practical significance**

940   Considered together, our results suggest that the mechanisms of P retention by biochar

941   made from sewage sludge, although homogeneous and reproducible at the macroscale,

942   will be highly heterogeneous at the micro and nanoscale and dependent on: (1)

943   feedstock composition, in particular Fe and Al concentration (but also Ca and Mg); (2)

944   pyrolysis conditions, where these affect the solubility of the mineral elements formed

945   during the process; (3) the reactivity of the chemical elements released from the soluble

946   mineral elements into solution during the P sorption/capture process; (4) the pH of the

947   system, as this directly affects (3); and (5) the concentration of phosphate in solution as

948   this will shift the equilibrium of the reaction, which has a similar activation energy in

949   the forwards and backwards directions (Barrow, 2015).

950

951 This study has shown that pelletisation of sewage sludge leads to retention of elements

952 within the biochar structure and/or contamination from the pelletising process compared

953 to non-pelletised sewage sludge. This is a positive feature for retention of nutrients, but

954 could lead to retention of potentially toxic elements (PTEs) inhibiting the environmental

955 suitability of biochar.

956

957 Our results also highlight the importance of minerals within the biochar structure for

958 their observed functionality in soil. When added to soil to improve soil quality in some

959 way, biochar mineral composition should be considered in combination with the

960 nutrient status of the biochar and the soil, as well as pH, in order to predict the effect on

961 nutrient mobility in the system. The PZC of the different minerals is an important

962 aspect, as this will dictate whether the mineral surfaces will be positively or negatively

963 charged at the native pH of the biochar, controlling the interactions between these

964 phases in biochar and nutrients or PTEs. The pH of the environment into which biochar

965 is added will also have an effect on this, so it is important to consider when tailoring a

966 biochar material to a specific purpose.

967

968 **5. Conclusions**

969 Sustainably produced biochar prepared from pelletised digested sewage sludge has an

970 affinity for P in solution higher than activated carbon and thus potential for P capture

971 and recycling. The inclusion of goethite-containing ochre as a minor ingredient prior to

972 sludge prior to pelletising and pyrolysis results in biochar that captures more P than

973 pelletised biochar from sludge only. Based on correlation analysis and surface

974 examination, Fe and Al present in complex mineral phases containing also Si, Mg and

975 Ca explained the P capture properties. Pyrolysis yields a greater proportion of less

976 soluble Fe/S minerals at 550°C than at 450°C, which may result in lower P capture over

977 the long term.

978

987

988 **References**

989 Ainsworth, C.C., Sumner, M.E., Hurst, V.E., 1985. Effect of Aluminum Substitution in

990   Goethite on Phosphorus Adsorption: I. Adsorption and Isotopic Exchange. Soil

991   Sci. Soc. Am. J. 49, 1142–1149. doi:10.2136/sssaj1985.03615995004900050015x

992 Angst, T.E., Sohi, S.P., 2013. Establishing release dynamics for plant nutrients from

993   biochar. GCB Bioenergy 5, 221–226. doi:10.1111/gcbb.12023

994 Arai, Y., Sparks, D.L., 2001. ATR–FTIR Spectroscopic Investigation on Phosphate

995   Adsorption Mechanisms at the Ferrihydrite–Water Interface. J. Colloid Interface

996   Sci. 241, 317–326. doi:10.1006/jcis.2001.7773

997 Arshadi, M., Zandi, H., Akbari, J., Shameli, A., 2015. Ferrocene functionalized

998   nanoscale mixed-oxides as a potent phosphate adsorbent from the synthetic and

999   real (Persian Gulf) waters. J. Colloid Interface Sci. 450, 424–433.

1000   doi:10.1016/j.jcis.2015.03.026

1001   Barrow, N.J., 2015. Soil phosphate chemistry and the P-sparing effect of previous

1002   phosphate applications. Plant Soil 397, 401–409. doi:10.1007/s11104-015-2514-5

1003   Barrow, N.J., 1983. A mechanistic model for describing the sorption and desorption of

1004   phosphate by soil. Eur. J. Soil Sci. 66, 9–18. doi:10.1111/ejss.12198

1005   Bhatnagar, A., Sillanpää, M., 2011. A review of emerging adsorbents for nitrate

1006   removal from water. Chem. Eng. J. doi:10.1016/j.cej.2011.01.103

1007   Buss, W., Graham, M., Shepherd, J.G., Masek, O., 2016a. Suitability of marginal

1008   biomass-derived biochars for soil amendment. Sci. Total Environ. 547, 314–322.

1009   doi:10.1016/j.scitotenv.2015.11.148

1010   Buss, W., Graham, M.C., Shepherd, J.G., Mašek, O., 2016b. Suitability of marginal

1011   biomass-derived biochars for soil amendment. Sci. Total Environ. 547, 314–322.

1012   doi:10.1016/j.scitotenv.2015.11.148

1013   Campbell, A., Schwertmann, U., Campbell, P., 1997. Formation of cubic phases on

1014   heating ferrihydrite. Clay Miner. 32, 615–622. doi:10.1180/claymin.1997.032.4.11

1015   Carr, S., 2012. An Investigation into Phosphorus Removal by Iron Ochre for the

1016   Potential Treatment of Aquatic Phosphorus Pollution. The University of

1017   Edinburgh.

1018   Chen, B., Chen, Z., Lv, S., 2011. A novel magnetic biochar efficiently sorbs organic

1019   pollutants and phosphate. Bioresour. Technol. 102, 716–723.

1020   doi:10.1016/j.biortech.2010.08.067

1021   Cornell, R.M., Schwertmann, U., 1996. The iron oxides: Structure, properties, reactions,

1022   occurrence and uses, 1st ed. VCH, Weinheim.

1023   Cucarella, V., Zaleski, T., Mazurek, R., Renman, G., 2008. Effect of reactive substrates

1024   used for the removal of phosphorus from wastewater on the fertility of acid soils.

1025   Bioresour. Technol. 99, 4308–4314. doi:10.1016/j.biortech.2007.08.037

1026   Dobbie, K.E., Heal, K. V., Aumônier, J., Smith, K. a., Johnston, a., Younger, P.L.,

1027   2009. Evaluation of iron ochre from mine drainage treatment for removal of

1028   phosphorus from wastewater. Chemosphere 75, 795–800.

1029   doi:10.1016/j.chemosphere.2008.12.049

1030   Downie, A., Crosky, A., Munroe, P., 2009. Physical Properties of Biochar, in:

1031   Lehmann, J., Joseph, S. (Eds.), Biochar for Environmental Management: Science

1032   and Technology. Earthscan, London, pp. 13–32.

1033   Drizo, A., Forget, C., Chapuis, R.P., Comeau, Y., 2006. Phosphorus removal by electric

1034   arc furnace steel slag and serpentinite. Water Res. 40, 1547–1554.

1035   doi:10.1016/j.watres.2006.02.001

1036   Enders, A., Lehmann, J., 2012. Comparison of Wet-Digestion and Dry-Ashing Methods

1037   for Total Elemental Analysis of Biochar. Commun. Soil Sci. Plant Anal. 43, 1042–

1038   1052. doi:10.1080/00103624.2012.656167

1039   Fang, L., Huang, L., Holm, P.E., Yang, X., Hansen, H.C.B., Wang, D., 2015. Facile

1040   upscaled synthesis of layered iron oxide nanosheets and their application in

1041   phosphate removal. J. Mater. Chem. A 3, 7505–7512. doi:10.1039/C4TA07083F

1042   Goldberg, S., Sposito, G., 1985. On the mechanism of specific phosphate adsorption by

1043   hydroxylated mineral surfaces: A review. Commun. Soil Sci. Plant Anal. 16, 801–

1044   821. doi:10.1080/00103628509367646

1045   Greenop, R., Wentworth, J., 2014. Phosphate Resources. UK Parliamentary Office of

1046   Science and Technology. POSTnote 477.

1047   Gull, M., Zhou, M., Fernández, F.M., Pasek, M.A., 2014. Prebiotic phosphate ester

1048   syntheses in a deep eutectic solvent. J. Mol. Evol. 78, 109–117.

1049   doi:10.1007/s00239-013-9605-9

1050   Hale, S.E., Alling, V., Martinsen, V., Mulder, J., Breedveld, G.D., Cornelissen, G.,

2013. The sorption and desorption of phosphate-P, ammonium-N and nitrate-N in

cacao shell and corn cob biochars. Chemosphere 91, 1612–1619.

doi:10.1016/j.chemosphere.2012.12.057

Heller-Kallai, L., Miloslavski, I., Aizenshtat, Z., Halicz, L., 1988. Chemical and mass

spectrometric analysis of volatiles derived from clays. Am. Mineral. 73, 376–382.

Hollister, C.C., Bisogni, J.J., Lehmann, J., 2013. Ammonium, Nitrate, and Phosphate

Sorption to and Solute Leaching from Biochars Prepared from Corn Stover (Zea

mays L.) and Oak Wood (Quercus spp.). J. Environ. Qual. 42, 137–44.

doi:10.2134/jeq2012.0033

IBI, 2012. Standardized Product Definition and Product Testing Guidelines for Biochar

That Is Used in Soil. International Biochar Initiative (IBI).

Joseph, S., Graber, E.R., Chia, C., Munroe, P., Donne, S., Thomas, T., Nielsen, S.,

Marjo, C., Rutlidge, H., Pan, G., Li, L., Taylor, P., Rawal, A., Hook, J., 2013.

Shifting paradigms: development of high-efficiency biochar fertilizers based on

nano-structures and soluble components. Carbon Manag. 4, 323–343.

doi:10.4155/cmt.13.23

Laird, D., Rogovska, N., 2015. Biochar Effects on Nutrient Leaching, in: Lehmann, J.,

Joseph, S. (Eds.), Biochar for Environmental Management, Science, Technology

and Implementation. Routledge, Oxon, pp. 521–542.

Li, J., Lv, G., Bai, W., Liu, Q., Zhang, Y., Song, J., 2016. Modification and use of

biochar from wheat straw (Triticum aestivum L.) for nitrate and phosphate removal

from water. Desalin. Water Treat. 57, 4681–4693.

doi:10.1080/19443994.2014.994104

Littler, J., Geroni, J.N., Sapsford, D.J., Coulton, R., Griffiths, A.J., 2013. Mechanisms

of phosphorus removal by cement-bound ochre pellets. Chemosphere 90, 1533–

1076   1538. doi:10.1016/j.chemosphere.2012.08.054

1077 Magdziarz, A., Wilk, M., 2013. Thermal characteristics of the combustion process of

1078   biomass and sewage sludge. J. Therm. Anal. Calorim. 114, 519–529.

1079   doi:10.1007/s10973-012-2933-y

1080 Mallet, M., Barthélémy, K., Ruby, C., Renard, A., Naille, S., 2013. Investigation of

1081   phosphate adsorption onto ferrihydrite by X-ray Photoelectron Spectroscopy. J.

1082   Colloid Interface Sci. 407, 95–101. doi:10.1016/j.jcis.2013.06.049

1083 Morales, M.M., Comerford, N., Guerrini, I. a., Falcão, N.P.S., Reeves, J.B., 2013.

1084   Sorption and desorption of phosphate on biochar and biochar-soil mixtures. Soil

1085   Use Manag. 29, 306–314. doi:10.1111/sum.12047

1086 Mukherjee, A., Zimmerman, A.R., Harris, W., 2011. Surface chemistry variations

1087   among a series of laboratory-produced biochars. Geoderma 163, 247–255.

1088   doi:10.1016/j.geoderma.2011.04.021

1089 Namasivayam, C., Sangeetha, D., 2004. Equilibrium and kinetic studies of adsorption of

1090   phosphate onto ZnCl2 activated coir pith carbon. J. Colloid Interface Sci. 280,

1091   359–65. doi:10.1016/j.jcis.2004.08.015

1092 Onay, O., Kockar, O.M., 2003. Slow, fast and flash pyrolysis of rapeseed. Renew.

1093   Energy 28, 2417–2433. doi:10.1016/S0960-1481(03)00137-X

1094 Parfitt, R., 1989. Phosphate reactions with natural allophane, ferrihydrite and goethite.

1095   J. Soil Sci. 40, 359–369. doi:10.1111/j.1365-2389.1989.tb01280.x

1096 Parfitt, R.., Russell, J.., 1977. Adsorption on hydrous oxides. IV. mechanisms of

1097   adsorption of various ions on goethite. J. Soil Sience 28, 297–305.

1098 Parfitt, R.L., Atkinson, R.J., Smart, R.S.C., 1975. The Mechanism of Phosphate

1099   Fixation by Iron Oxides. Soil Sci. Soc. Am. 39, 838–841.

1100   doi:10.2136/sssaj1975.03615995003900050017x

1101 Park, J.H., Ok, Y.S., Kim, S.H., Cho, J.S., Heo, J.S., Delaune, R.D., Seo, D.C., 2015.

1102 Evaluation of phosphorus adsorption capacity of sesame straw biochar on aqueous

1103 solution: influence of activation methods and pyrolysis temperatures. Environ.

1104 Geochem. Health 37, 969–983. doi:10.1007/s10653-015-9709-9

1105 Qiu, Y., Zheng, Z., Zhou, Z., Sheng, G.D., 2009. Effectiveness and mechanisms of dye

1106 adsorption on a straw-based biochar. Bioresour. Technol. 100, 5348–5351.

1107 doi:10.1016/j.biortech.2009.05.054

1108 Rawal, A., Joseph, S.D., Hook, J.M., Chia, C.H., Munroe, P.R., Donne, S.W., Lin, Y.,

1109 Phelan, D., Richard, D., Mitchell, G., Pace, B., Horvat, J., Beau, J., Webber, W.,

1110 2016. Mineral-Biochar Composites: Molecular Structure and Porosity. Environ.

1111 Sci. Technol. 50, 7706–7714. doi:10.1021/acs.est.6b00685

1112 Reddy, K.R., Kadlec, R.H., Flaig, E., Gale, P.M., 1999. Phosphorus retention in streams

1113 and wetlands: a review. Crit. Rev. Environ. Sci. Technol. 29, 83–146.

1114 doi:10.1080/10643389991259182

1115 Reijnders, L., 2014. Resources , Conservation and Recycling Phosphorus resources ,

1116 their depletion and conservation , a review. "Resources, Conserv. Recycl. 93, 32–

1117 49. doi:10.1016/j.resconrec.2014.09.006

1118 Ren, J., Li, N., Li, L., An, J.-K., Zhao, L., Ren, N.-Q., 2015. Granulation and ferric

1119 oxides loading enable biochar derived from cotton stalk to remove phosphate from

1120 water. Bioresour. Technol. 178, 119–125. doi:10.1016/j.biortech.2014.09.071

1121 RStudio Team, 2015. RStudio: Integrated Development for R.

1122 Sakadevan, K., Bavor, H.J., 1998. Phosphate adsorption characteristics of soils, slags

1123 and zeolite to be used as substrates in constructed wetland systems. Water Res. 32,

1124 393–399. doi:10.1016/S0043-1354(97)00271-6

1125 Schneider, F., Haderlein, S.B., 2016. Potential effects of biochar on the availability of

1126   phosphorus — mechanistic insights. Geoderma 277, 83–90.

1127   doi:10.1016/j.geoderma.2016.05.007

1128 Shepherd, J.G., Sohi, S.P., Heal, K.V., 2016. Optimising the recovery and re-use of

1129   phosphorus from wastewater effluent for sustainable fertiliser development. Water

1130   Res. 94, 155–165. doi:10.1016/j.watres.2016.02.038

1131 Sibrell, P.L., Montgomery, G. a., Ritenour, K.L., Tucker, T.W., 2009. Removal of

1132   phosphorus from agricultural wastewaters using adsorption media prepared from

1133   acid mine drainage sludge. Water Res. 43, 2240–2250.

1134   doi:10.1016/j.watres.2009.02.010

1135 Silber, A., Levkovitch, I., Graber, E.R., 2010. PH-dependent mineral release and surface

1136   properties of cornstraw biochar: Agronomic implications. Environ. Sci. Technol.

1137   44, 9318–9323. doi:10.1021/es101283d

1138 Steenari, B., Lindqvist, O., 1998. High Temperature Reactions of Straw Ash and the

1139   Anti-Sintering Additives Kaolin and Dolomite. Biomass and Bioenergy 14, 67–76.

1140 Steffen, W., Richardson, K., Rockström, J., Cornell, S., Fetzer, I., Bennett, E., Biggs,

1141   R., Carpenter, S.R., de Wit, C. a., Folke, C., Mace, G., Persson, L.M.,

1142   Veerabhadran, R., Reyers, B., Sörlin, S., 2015. Planetary Boundaries: Guiding

1143   human development on a changing planet. Science 347.

1144   doi:10.1126/science.1259855

1145 Streubel, J.D., Collins, H.P., Tarara, J.M., Cochran, R.L., 2012. Biochar Produced from

1146   Anaerobically Digested Fiber Reduces Phosphorus in Dairy Lagoons. J. Environ.

1147   Qual. 41, 1166. doi:10.2134/jeq2011.0131

1148 Torrent, J., Schwertmann, U., Barrón, V., 1992. Fast and slow phosphate sorption by

1149   goethite-rich natural materials. Clays Clay Miner. 40, 14–21.

1150   doi:10.1346/CCMN.1992.0400103

1151   Wang, Z., Nie, E., Li, J., Yang, M., Zhao, Y., Luo, X., Zheng, Z., 2012. Equilibrium

1152   and kinetics of adsorption of phosphate onto iron-doped activated carbon. Environ.

1153   Sci. Pollut. Res. 19, 2908–2917. doi:10.1007/s11356-012-0799-y

1154   Yao, Y., Gao, B., Inyang, M., Zimmerman, A.R., Cao, X., Pullammanappallil, P., Yang,

1155   L., 2011. Biochar derived from anaerobically digested sugar beet tailings:

1156   Characterization and phosphate removal potential. Bioresour. Technol. 102, 6273–

1157   6278. doi:10.1016/j.biortech.2011.03.006

1158   Yao, Y., Gao, B., Zhang, M., Inyang, M., Zimmerman, A.R., 2012. Effect of biochar

1159   amendment on sorption and leaching of nitrate, ammonium, and phosphate in a

1160   sandy soil. Chemosphere 89, 1467–1471. doi:10.1016/j.chemosphere.2012.06.002

1161   Zhang, H., Chen, C., Gray, E.M., Boyd, S.E., Yang, H., Zhang, D., 2016. Roles of

1162   biochar in improving phosphorus availability in soils: A phosphate adsorbent and a

1163   source of available phosphorus. Geoderma 276, 1–6.

1164   doi:10.1016/j.geoderma.2016.04.020

1165   Zhang, M., Gao, B., Yao, Y., Inyang, M., 2013. Phosphate removal ability of

1166   biochar/MgAl-LDH ultra-fine composites prepared by liquid-phase deposition.

1167   Chemosphere 92, 1042–1047. doi:10.1016/j.chemosphere.2013.02.050

1168   Zhang, M., Gao, B., Yao, Y., Xue, Y., Inyang, M., 2012. Synthesis of porous MgO-

1169   biochar nanocomposites for removal of phosphate and nitrate from aqueous

1170   solutions. Chem. Eng. J. 210, 26–32. doi:10.1016/j.cej.2012.08.052

1171